atmosphere

Review

Study of the Mesosphere and Lower Thermosphere by the Method of Creating Artificial Periodic Irregularities of the Ionospheric Plasma

Nataliya V. Bakhmetieva * and Gennadiy I. Grigoriev

Radiophysical Research Institute, Nizhny Novgorod State University, 25/12a Bol'shaya Pecherskaya Str., 603950 Nizhny Novgorod, Russia
* Correspondence: nv_bakhm@nirfi.unn.ru

Abstract: This article presented a brief review of studies of the Earth's ionosphere at the heights of the mesosphere and lower thermosphere by a method based on the creation of artificial periodic inhomogeneities (APIs) of the ionospheric plasma by high-frequency radiation from powerful thermal installations. APIs are created by a standing wave due to the interference between upward-propagating radio waves and those reflected from the ionosphere. API studies of the ionosphere were based on Bragg scattering of probing impulse signals from an artificial periodic structure. The method makes it possible to measure the parameters of the neutral and ionized components of the Earth's atmosphere. Note that, despite the fact that the API method assumes an artificial perturbation of the ionospheric plasma, the parameters of the mesosphere and lower thermosphere are determined at the stage of inhomogeneity relaxation and characterize the undisturbed medium. To date, periodic inhomogeneities have been observed at the heating points of Zimenki and Sura ionospheric heating facility (SURA, Vasilsursk, Russia), Gissar (Tajikistan), Arecibo (Puerto Rico, USA), High Power Auroral Stimulation Observatory (HIPAS) and High Frequency Active Auroral Research Program (HAARP, Gakona, AK, USA), and European Incoherent Scatter (EISCAT, Tromso, Norway). Most of the API studies of the ionosphere were carried out at the SURA mid-latitude heating facility (56.1° N; 46.1° E). The review presented the main results of determining the parameters of the ionosphere and neutral atmosphere at altitudes of 60–120 km and studies of the atmosphere during sunrise and sunset events and solar eclipses. In fact, the review is far from a complete illustration of the possibilities of using the API method to study the mesosphere and lower thermosphere.

Keywords: ionosphere; mesosphere; lower thermosphere; artificial periodic irregularities; electron density; neutral temperature; plasma velocity; turbulence; sporadic E layer; waves

check for updates

Citation: Bakhmetieva, N.V.; Grigoriev, G.I. Study of the Mesosphere and Lower Thermosphere by the Method of Creating Artificial Periodic Irregularities of the Ionospheric Plasma. *Atmosphere* **2022**, *13*, 1346. https://doi.org/10.3390/atmos13091346

Academic Editors: Chen Zhou and Zhibin Yu

Received: 1 August 2022
Accepted: 17 August 2022
Published: 24 August 2022

Publisher's Note: MDPI stays neutral with regard to jurisdictional claims in published maps and institutional affiliations.

1. Introduction

In the second half of the 20th century, traditional methods for studying the ionosphere were significantly expanded through the use of active experiments in space (ionosphere). Under this name, studies related to the purposeful reversible change of certain properties of the ionosphere are combined. Among other things, they include the impact on the ionospheric plasma by powerful radiation from ground-based HF radio transmitters or heating facilities. One of these relatively new methods is a method based on the creation of artificial periodic irregularities of the ionospheric plasma.

The first ideas about the generation of periodic irregularities in the lower ionosphere by powerful radio waves were created by Vilensckii's group in 1970 [1]. They assumed that APIs are due to electron temperature irregularities. The first API observation in the F region of the ionosphere was carried out by Belikovich et al. using the Zimenki heating facility (56.16° N; 44.3° E) in 1975 [2]. Furthermore, APIs were observed at the heating facilities at Arecibo [3], HIPAS [4], EISCAT [5–7], and HAARP [8–10]. During the period of active research on this phenomenon, the physical processes that cause the formation of periodic inhomogeneities in the field of a powerful standing wave were considered. On this basis, methods were developed for determining a number of parameters of the ionosphere and neutral atmosphere. These methods were applied in studies conducted at the SURA heating facility [11].

The theory of the formation and relaxation of irregularities and the results of many years of research into the ionosphere by the API technique until 2000 are summarized in the monograph [11]. In this review, the main attention is paid to the results of the studies of the ionosphere by the API method obtained using the SURA heating facility after 2000. The API technique is based on the disturbance of the ionosphere by powerful high-frequency radio emission with the creation of periodic irregularities in the field of a standing wave formed by reflection from the ionosphere of a powerful radio wave emitted at the zenith by a heating facility. Irregularities are formed in the altitude range from 50 km to the height of reflection of powerful waves from the ionosphere. The scheme for the API formation is shown in Figure 1.

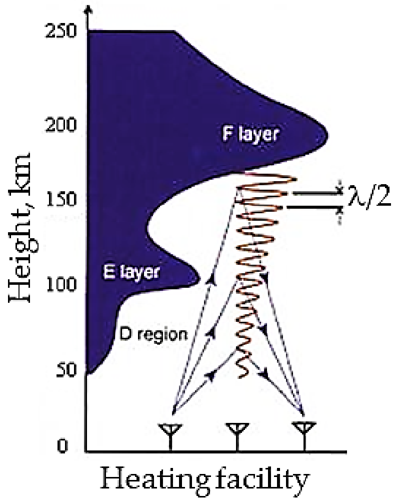

Figure 1. Scheme for API formation by powerful heating facility radiation and probing. After [11].

The main features of the API formation are detailed in [11]. Note that, in different regions of the ionosphere, the formation of irregularities is caused by different physical processes. In the D region (height of 60–90 km), the temperature dependence of the coefficient of electron attachment to neutral molecules plays a key role in the API formation. In the E region (altitude of 90–150 km), APIs are formed due to the diffusion redistribution of plasma under the action of an excess pressure of the electron gas, while in the F region (altitude of 150–350 km), APIs arise under the action of a ponder motive force on the ionospheric plasma. The vertical scale of irregularities is equal to half the wavelength in the plasma emitted by the transmitters of the heating facility. The study of the ionosphere and neutral atmosphere by the API method was based on the observation of Bragg backscattering of pulsed probing radio waves on periodic irregularities and the measurement of the amplitude and phase of the scattered signal. We have developed more than ten methods for determining the parameters of the ionosphere and neutral atmosphere using this method. The API technique and methods for determining many parameters of the ionosphere are presented in detail [11].

The API technique makes it possible to obtain many parameters at the mesosphere and lower thermosphere heights. We note the main ones:

- Electron density profiles in the E region, including the interlayer E–F valley;
- The vertical plasma velocity;
- The neutral component velocity in the mesosphere and lower thermosphere (60–130 km);
- Turbulent velocity and turbo pause level;
- Temperature and density of the neutral atmosphere at the E region heights (90–120 km);

- Molecular masses and densities of prevailing metal ions in the sporadic-E layer;
- Relative concentration of negative ions of oxygen, concentration of atomic oxygen, and raised molecular oxygen $^1\Delta_g$ in the D region;
- Electron and ion temperatures in the F region.

The API technique allows us to study many natural phenomena in the lower ionosphere including the sporadic E layer and its ion composition, internal gravity wave parameters, neutral atmosphere turbulence, irregular structure of the lower ionosphere, and stratifications of the profile of the electron density from the heights in the D region to the maximum of the F region, sunset–sunrise phenomena in the lower ionosphere, terminator effect, and, in the lower ionosphere, the condition during a solar eclipse [12–23]. We presented the results of the studies of some of these phenomena in the following sections. In fact, the article is a rather complete illustration of the possibilities of the API method. Specific results with their detailed discussion can be found in the extensive list of references contained in the article. The methods to determine the electron concentration, neutral temperature and density ρ, turbulent velocity, and masses of the main ions in the sporadic E layer are based on the height dependence of the scattered signal relaxation time [24–26].

We now give an overview of the remaining sections of the article. Section 2 presents a brief description of a relatively new method for studying the Earth's ionosphere, including the mesosphere and lower thermosphere, and based on the creation of artificial periodic irregularities in the ionospheric plasma. Sections 3 and 4 include examples of determining several important parameters of the neutral and ionized components of the Earth's atmosphere at altitudes of 60–120 km. Section 5 discusses the possibilities of studying the features of the twilight ionosphere and the manifestation of a solar eclipse in the characteristics of scattered API signals. Finally, Section 6 provides the conclusions and outlines areas for future research.

2. API Technique and Experiment Description

For API formation, we used a powerful transmitter (heating facility) that creates electromagnetic field that disturbs the ionosphere plasma. At the seven heating facilities, APIs were observed in different years. At present, the SURA, HAARP, and EISCAT and heater facilities can be used for API monitoring.

2.1. Equipment and Methodic of the Experiment

Under certain conditions, APIs scatter probing radio waves incident on them. In order to record the parameters of the API scattered signal, receivers need pulse radar in the same frequency range as the heating transmitter. In the first years of the API study, we used the receiving part of the partial reflection setup. Now, the SURA heating facility is used as a source of both powerful and probe radio waves for API formation and their diagnostics. The transmitters of the SURA facility are used as radar in the pulsed mode of emitting probe radio waves. Using different time schemes for the emission of high-power and probe radio waves, it is possible to study the API rise and decay processes. A detailed description of the SURA facility and receiving part of the partial reflection setup, which is also used to receive API scattered signals, is given in [11,27,28].

Figure 2a schematically shows the time diagrams for studying API decay (relaxation). It implements a continuous heating mode for several (usually 2–3) seconds, followed by switching the heating facility to a pulsed diagnostic mode with the emission of short 30 μs pulses. The receiving unit receives the signal scattered by inhomogeneities and registers its amplitude and phase during the entire period of their relaxation. Figure 2b shows the time diagrams for studying API rise and decay. It shows heating 100 ms period pulse with short gaps in which the short 20 μs pulse is emitted to study the rise of irregularities.

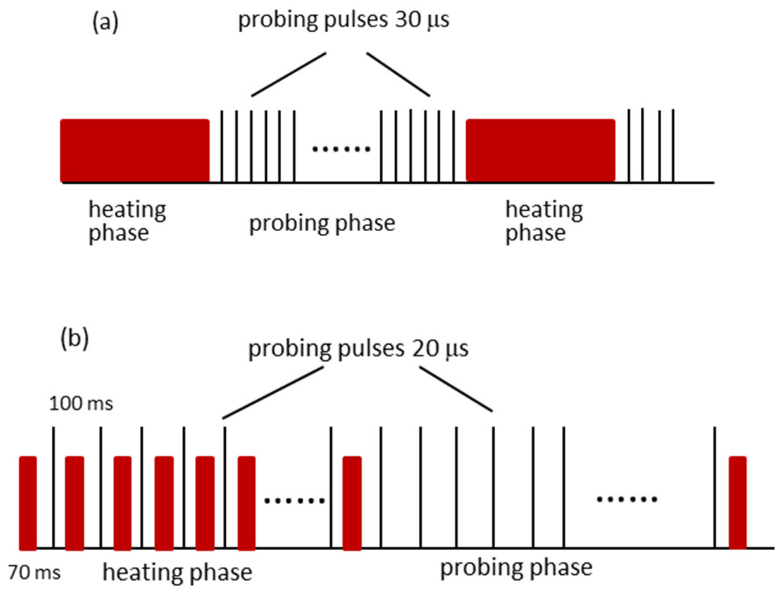

Figure 2. Two time schedules of SURA facility used for API formation and diagnostics: continuous heating (**a**) is used for API diagnostics on their decay (relaxation) stage and quasi-continuous heating (**b**) allows studying the process of API development.

When sounding of the periodic structure was performed with probe radio waves, the API scattered signal was received by the antenna system and receivers of the partial reflection facility located at a distance of 1 km from the heating facility. The amplitude and phase of the scattered signal were measured. The relaxation time of inhomogeneities was determined by decreasing the amplitude by a factor of e.

Figure 3a,b give an example of the API scattered signal parameters during their relaxation stage. The decrease in the amplitude of the API scattered signal with time in Figure 3a is visible as the rapidly periodic oscillation in the F region below the height of the specular reflection of high-power and probe radio waves (1) and a gradual decrease in the signal amplitude at altitudes of 60–140 km in the E region and sporadic E layer (2,3) and in the stratified D region (4).

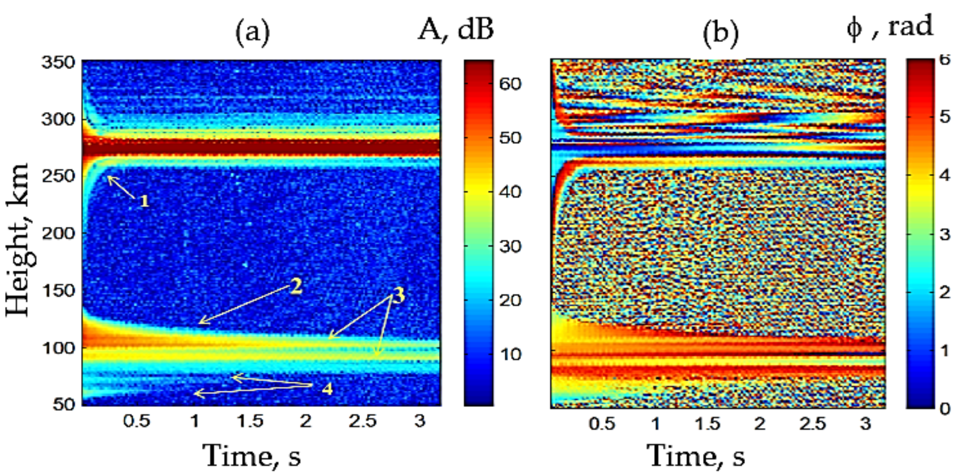

Figure 3. *Cont.*

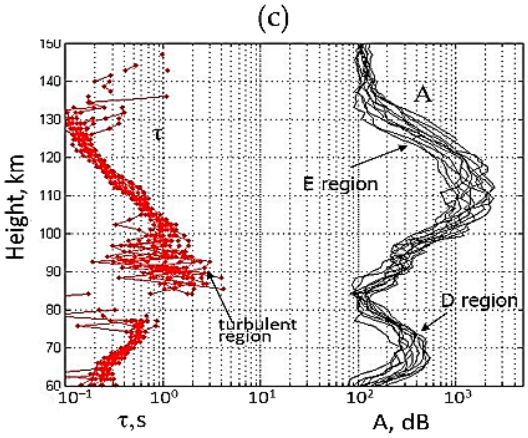

Figure 3. Typical example of API scattered signal recording in real time: height–time–amplitude plot *A* (**a**) and phase–time–amplitude plot *φ* (**b**) illustrating the API decay (relaxation) process; (**c**) height profiles of signal relaxation time (left panel) and amplitude (right panel). From [11,29].

Figure 3c gives an example of the height profiles of the scattered signal relaxation time τ and its amplitude A. The curves correspond to data averaged over 5 min at each height. In this example, the diffusion law of relaxation corresponds to a height interval of 100–120 km. The relaxation times are in good agreement with the diffusion dependence τ(h). Under a height of 100 km, atmospheric turbulence begins to have an effect, while the relaxation time of the scattered signal decreases. At an altitude of 85 km, a local increase in the amplitude of the scattered signal is ensured by an anomalously low sporadic E layer. A local maximum of the relaxation time is observed at the same height. For the heights of the D region, the amplitude and relaxation time change with height in full accordance with the temperature dependence of the electron detachment coefficient [11].

Figure 4a,c show two examples of the API scattered signal obtained in the recent experiments. Dependences of amplitude versus height on eight virtual heights are shown in Figure 4b,d. Figure 4a shows strong API echoes in the E region between 90 and 145 km. In the D region, API echoes were observed in the height range of 60–85 km. Their amplitudes are characterized by spatial and temporary variations. API signals in the E region reach the maximum amplitude at the height of 115 km. During the heating period, one can see the development of the API signal scattered in the F region in the altitude range of 160–270 km below the height of the specular reflection of the test radio wave. The horizontal stripes at the top of Figure 4a are specular reflections of the probe radio wave. Figure 4b,d show that the characteristic times of the API growth and decay are approximate. Relaxation or decay time is defined at e-times reduction of the amplitude of the scattered signal. In this example, the times of rise and decay in the E region reached 1–1.5 s. These values of API time scales are typical for the E region when the ambipolar diffusion dominates in the formation and relaxation of the API [11]. The F-region API echoes evolved and disappear usually less than 30–300 ms after the heater switching on and off. Figure 4c gives an example of an intense scattered signal in the D region during the development of an intensive sporadic layer E, which is visible in the figure at a height of 100–120 km. After the end of the impact on the ionosphere, the scattered signal in the D region during the API relaxation process existed for almost 3 s. Very weak scattered signals existed at that time in the F region as a result of the reflection of a powerful wave of the forming API mainly from the E_s layer.

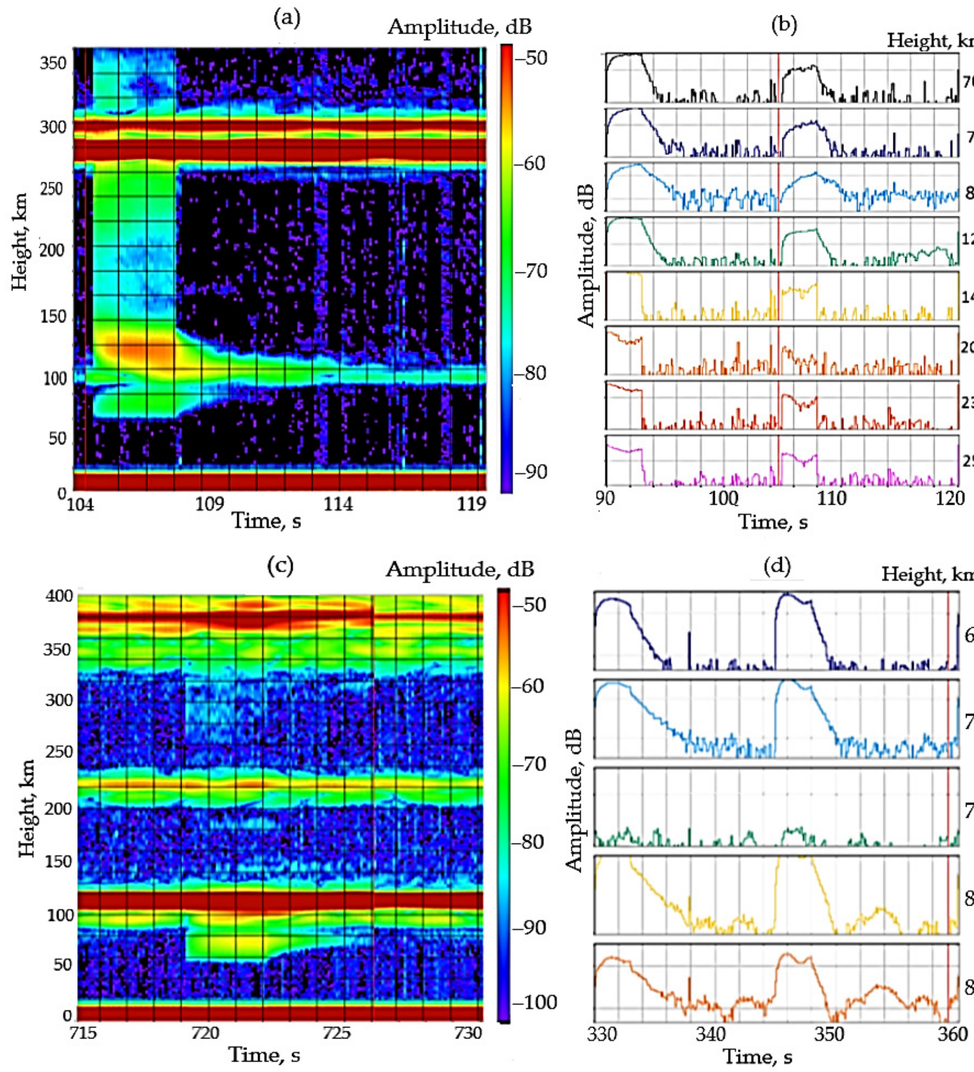

Figure 4. Height–time–amplitude plots illustrating the API rise and decay from 2 September 2021 at 16:48 LT (**a**) and 12:50 LT (**c**). Amplitudes of API scattered signal at the six heights from 70 to 250 km (**b**) and from 65 to 85 km (**d**) for two sessions of the observation.

This review is not a discussion of the processes of development and relaxation of inhomogeneities and their features depending on ionospheric conditions. Here, we will focus on presenting the results of applying the API technique to the measurement of some parameters of the mesosphere and lower thermosphere. This is one of the most important aspects of the application of the API method.

2.2. The Method for Determining the Ionized and Neutral Components

In this review, we gave only a brief description of the basics of the method. The physical processes in the ionosphere leading to the formation of periodic inhomogeneities were discussed in detail in [11]. When using the API technique, it is important to note that the scattering at the API has a resonant character. An intense scattered signal occurs only when the wave scattered by individual irregularities is in phase. If the heating and probing facilities are in the location, the condition of the resonance is equality of the powerful λ_1 and probing wave λ_2 in plasma. It is the Bragg scattering condition. This condition is automatically met at all altitudes if the signals of the same frequency and polarization are used for creating and probing irregularities. In the case when radio waves of different frequencies and polarizations are used to create and locate inhomogeneities, they should be related by the relation $f_1 n_1^{o,x} = f_2 n_2^{x,o}$, where f_1 and f_2 are the frequencies of the powerful and probing radio waves, and n_1 and n_2 are the refractive indices of the different magnetoionic modes. As refractive indices depend on the electron density, this equality appears as an equation combining f_1 and f_2 frequencies with the plasma and electron gyro frequencies. The correct selection of operating frequencies makes it possible to measure the electron density at heights where this relation is satisfied. We called this method of API creation and diagnostics as the two-frequency technique [11,15,17,25]. We used both of the variants of the API technique implementation for determining many parameters of the ionosphere and neutral atmosphere.

3. API Technique and the Ionized Component Parameters

3.1. N(h)-Profile

The main feature of the API technique is the possibility to measure the height profile of the electron density N(h) in the ionosphere including the valley between the E and F layers. An example of implementation of the two-frequency technique for N(h) profile measurements is shown in Figure 5a. Note that the N(h) profiles have varied over time. Initially, profiles were uniform and electron density smoothly increased with height. Then the valley appeared between 120 and 140 km, and later, a more detailed irregular structure in the valley region developed including sporadic E layers at the height of 115 km and an intermediate layer in the valley of 145 km. Figure 5b shows an example of N(h) with the interlayer valley between 115 and 153 km and two sporadic E layers at 98 and 130 km.

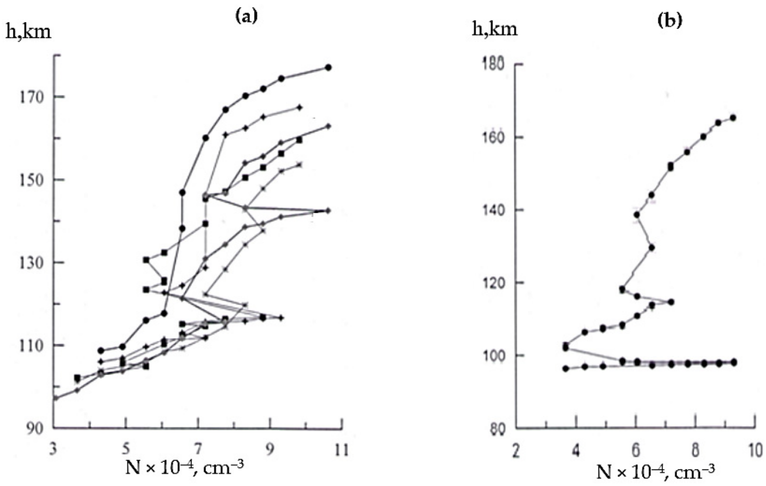

Figure 5. Electron density profiles obtained on 17 December 1991 for time from 09:00 to 12:35 (**a**) and 4 October 1991 at 16:30 LT (**b**). Examples demonstrate electron density with sporadic E layers and intermediate layers in the E-F valley. From [11,30].

Note, that the valley between the E and F layers is the least explored region of the ionosphere. To a large extent, the valley is controlled by the Sun zenith angle and wave processes leading to the formation of multiple E_s layers and stratification of the E layer [31,32]. We often observed similar layering in the E region, including the E_s layer, by the API technique. An example of the layered structure of the E region is shown in Figure 6a. We believe that the splitting is apparently caused by the interference of the signals scattered by API, sporadic E layers, and large-scale ionospheric irregularities.

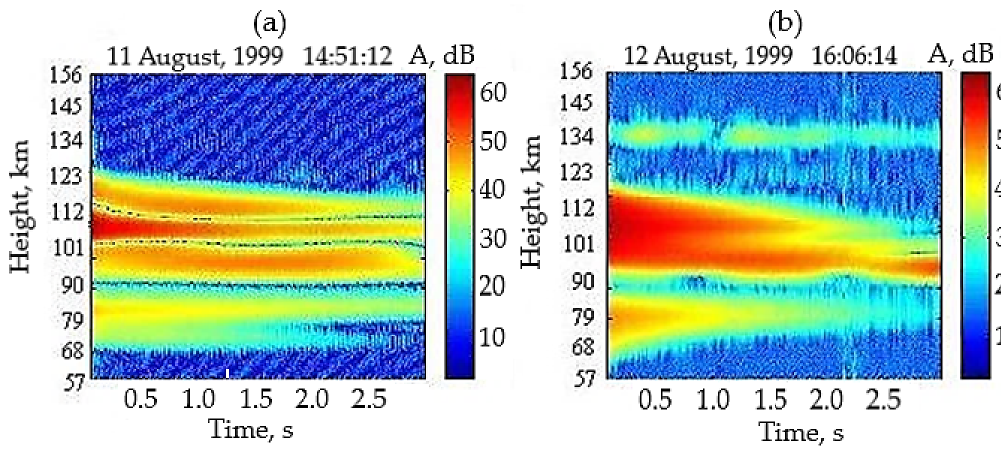

Figure 6. Time–height–intensity plot of the API scattered signal, including the period of the solar eclipse on 11 August 1999 (**a**) and the next day 12 August 1999 (**b**). These are examples of the complex structure of the E region during eclipse (**a**) and the stratification of the sporadic E layer (**b**). Similar layered structures have often been observed during eclipses and other ionospheric disturbances. From [30].

Many studies considered the interaction of regions E and F during the propagation of medium-scale traveling ionospheric disturbances (TIDs), as well as the influence of solar thermal tidal motions that cause the appearance of the so-called descending intermediate E_s layers [33–35]. A feature of the intermediate E_s layers is the appearance at heights between the E and F regions and a further downward movement toward the E region. It seems that, in Figure 6b, the signal at 135 km is the scattering from the intermediate E_s.

We obtained many $N(h)$ profiles using the two-frequency API technique [17]. According to the height dependence, they can be classified into several main types. Figure 7a shows ordinary $N(h)$ profiles, most often observed in the near-noon hours. They are characterized by smooth dependence $N(h)$, which is close to regular E-region models. Figure 7b shows electron density profiles with pronounced sporadic E layers. Figure 7c,d show profiles with irregular variations in the electron density by stratifications near the layer maximum and profiles for those with wave-like variations in the electron density versus height.

On the basis of the above examples of determining the electron density in the E region of the ionosphere based on the results of the API creation by the two-frequency method, we can conclude the following. The method makes it possible to obtain both smooth standard profiles and observe the fine structure (stratifications) of the E region. The electron density profiles obtained by this new method demonstrate all the main features of the electron density at these heights. Sporadic layers are observed, including weak, inaccessible ionosonde registrations. There are dynamic phenomena associated with waves, turbulent formations, etc.

3.2. APIs and Sporadic E Layers

The layers of increased ionization that appear at the heights of the E region of the ionosphere are called sporadic E layers (E_s layers). These sporadic layers in the E region, which occur at all latitudes, have been studied for many decades. Most of the information we have about E_s layers comes from vertical sounding with ionosondes, but weak cloud layers are not visible for them. The application of the API technique successfully solves this problem. Examples of scattered signals from weak sporadic layers can be seen in Figures 3 and 6b. Figure 4c shows the reflection from the intense E_s layer.

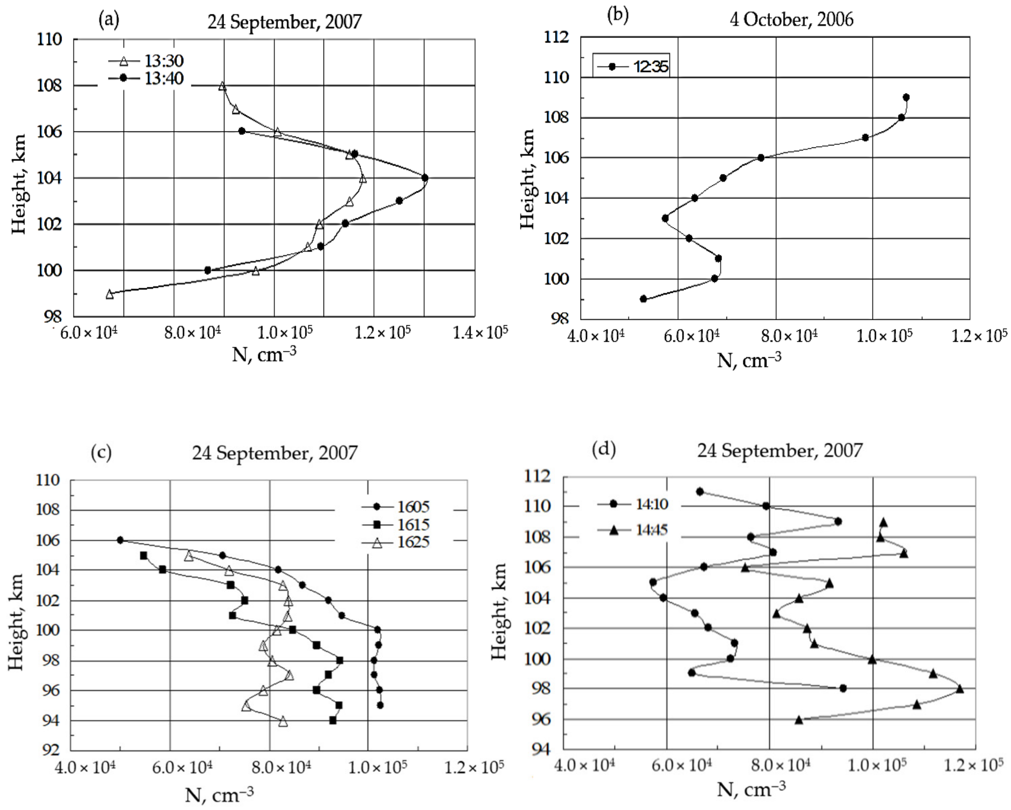

Figure 7. Some electron density profiles obtained on 24 September 2007 (**a**,**c**,**d**) and 4 October 2006 (**b**). Session times (LT) are indicated on the panels. From [28].

The effect of the sporadic E layer on the scattered signal is expressed in the local growth of its amplitude A(h) at the altitudes of the E_s layer, sometimes by 30–40 dB [18,25,36–41]. Obviously, this growth is due to an increase in the coefficient of the reflection of radio waves from the E_s layer, which is provided as an increase in the amplitude of the periodic inhomogeneities, and is proportional to the electron density in the layer, and an increase in the heating action of the standing wave due to the growth of its length (due to a decrease in the refractive index), reducing losses in energy electrons through thermal conductivity. Scattering of the radio waves by inhomogeneities of the natural semitransparent E_s layer also causes an increase in the amplitude of the signal, but the phase of the "natural" component differs from the phase of the signal scattered by periodic inhomogeneities. Phase differences allow us to separate the signals scattered from natural heterogeneities from those scattered by a periodic structure. Figure 8 gives an example of the influence of the E_s layer on the amplitude and relaxation time of the API scattered signal.

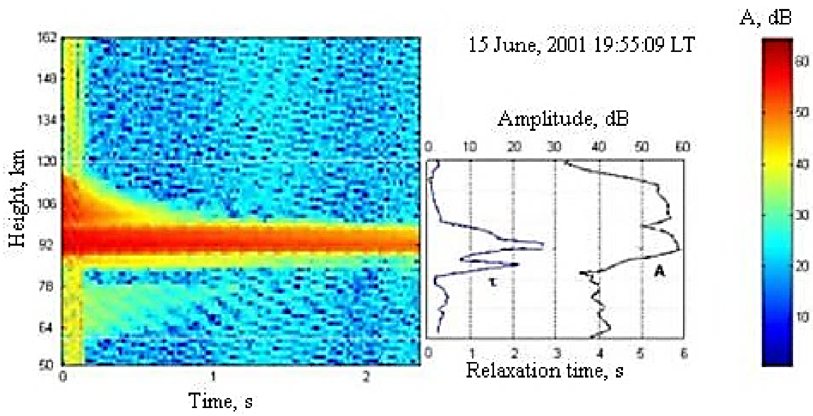

Figure 8. Example of influence of E_s layer on amplitude and relaxation time of API scattered signal.

The effect of the sporadic layer leads to an increase in the signal amplitude, and local maxima appear on the plot of the height dependence of the scattered signal relaxation time $\tau(h)$ at the height of the E_s layer. This observation is the basis for the method of determining the molecular weight of positive metal ions that predominate in the E_s layer [19,25,39].

In the E region, the API relaxation process is caused by ambipolar diffusion. In the absence of a sporadic E layer and turbulence, the height dependence of the relaxation time of the API $\tau(h)$ corresponds to the diffusion approximation in the lower thermosphere. In this event, the relaxation time τ of irregularities is given by the formula

$$\tau = \frac{1}{K^2 D} = \frac{M_i \nu_{im}}{k_B (T_{e0} + T_{i0}) K^2} = \frac{M_i \nu_{im}}{2\, k_B T K^2},$$

where k_B is the Boltzmann constant, $K = 4\pi/\lambda$ is the wavenumber of a standing wave, $\lambda = \lambda_0/n$ is the wavelength in plasma, n is the refractive index, D is the coefficient of ambipolar diffusion, M_i is the molecular mass of ions, T_{e0} and T_{i0} are the unperturbed values of electron and ion temperatures, respectively, and ν_{im} is the frequency of collisions of ions with neutral molecules. The ratio of the API relaxation times in its region and in the E_s layer is expressed by the formula $\frac{\tau_{Es}}{\tau} = (\frac{n_E}{n_{Es}})^2 \left(\frac{M_M \cdot \nu_{im}^M}{M_A \cdot \nu_{im}^A}\right)$, where τ and n_E are the diffusional relaxation time and refractive index in the background E region in the absence of the E_s layer, respectively, τ_{Es} and n_{Es} are the same characteristics at the height of the E_s layer, ν_{im}^M and ν_{im}^A are the collision frequencies of basic metal ions and main atmospheric ones with neutrals, respectively, and M_M and M_A are their masses. From the ratio of the relaxation time, it follows that the greatest impact on $\tau(h)$ should provide more heavy metal ions, for example, iron Fe^+ ions with an atomic mass $M_M = 56$ (which is almost twice the average molecular weight of atmospheric ions NO^+ ($M = 30$) and $O_2{}^+$ ($M = 32$) prevailing at the E-region altitude, or calcium ions Ca^+ ($M_M = 40$)). According to the results of the experiments during the years 2006–2014, descending E_s layers were found containing ions with masses 39 and 57 atomic units, which are close to the masses of the ions Ca^+ and Fe^+. For the E_s layer, observed near the maximum of the E region, the value $M_M = 37$ was obtained. This means that a certain percentage of the ions formed in the layer E_s can be lighter ions such as sodium ions $M_M = 23$, for example. The ion mass estimates obtained using the API method correspond to the results of measuring the ionic composition of the E_s layer [42,43].

Figure 9 shows the effect of the E_s layer on the amplitude and relaxation time of the API scattered signal. Influence manifests itself in the form of a significant increase in the amplitude and relaxation time of the scattered signal. Wave-like variations manifest themselves in temporal dependences of relaxation time.

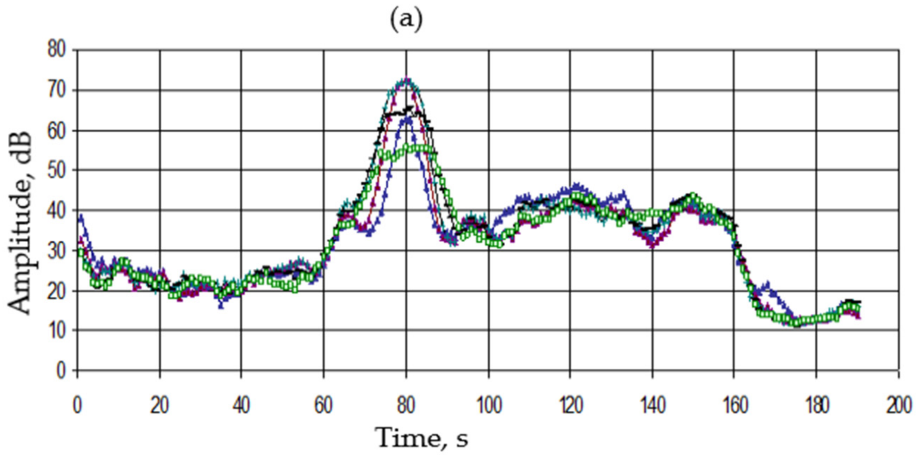

Figure 9. *Cont.*

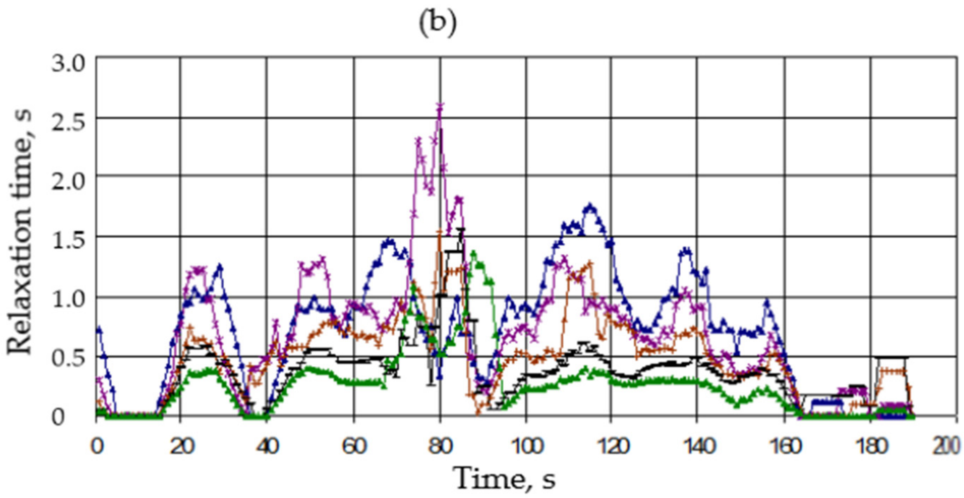

Figure 9. Amplitude (**a**) and relaxation time (**b**) of API scattered signal on several heights from 96.4 km to 107.4 km (represented by different colors) in lower thermosphere on 20 May 2010 at 18:05 LT. Influence of sporadic layer E on amplitude and relaxation time manifests itself in the form of a significant increase in the amplitude and relaxation time of the scattered signal. Wave-like variations manifest themselves in temporal dependences of relaxation time. From [39].

3.3. Ionization in the D Region

At the heights of the D region, the APIs are formed due to an increase in the rate of electron attachment to oxygen molecules, which leads to a decrease in the electron density and an increase in the number density of negative oxygen ions [11,12,21,24]. Experimental height profiles of the amplitude and decay time of the signals scattered by APIs exhibit a gradual increase up to a height of about 77 km. Above this level, the amplitude and decay time of the signal abruptly decrease, which is explained by the increase in the atomic oxygen density. The high density of atomic oxygen in the atmosphere leads to an increase in the total rate of electron detachment from negative ions, which almost destroys the API formation mechanism characteristic of the D region. In [21,24], experimental height profiles of the amplitude and decay time of the signals scattered by APIs in the daytime D layer are presented in detail and quantitatively explained on the basis of the model of photochemical processes involving a single negative ion species O_2^-.

Figure 10 shows multiple consecutive height profiles of the amplitude (a) and relaxation time (b) of the API scattered signal. Each profile is obtained by averaging data over 15 min.

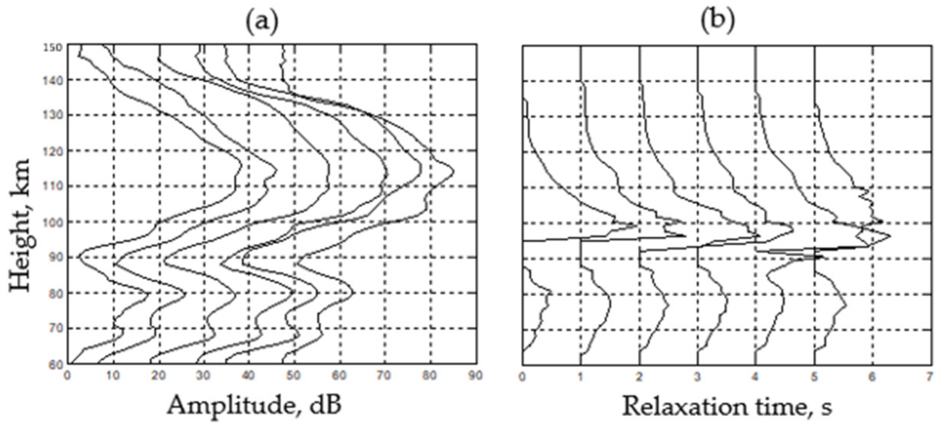

Figure 10. Series of height profiles of amplitude (**a**) and relaxation time (**b**) of API scattered signal on 6 April 2006 for 18:05 LT. From [30].

One can see the minimum amplitude of the scattered signal at a height of 72–74 km, which allows us to talk about stratification. Stratification occurs only in the height profile of the signal amplitude and is absent in the relaxation time profile. This is not a single observation; such profiles with stratification are obtained at different times of the year, but more often in the spring and autumn periods.

It is shown that the altitude profiles of the amplitude in the lower part are determined by the density of the atmosphere and in the upper part by the concentration of atomic oxygen [11]. In this case, the amplitude profile also depends on the height profile of the electron concentration. This suggests that the two-layer profile of the scattered signal amplitude manifests itself as a two-layer D region. Perhaps the bottom layer is layer C, which they try to detect with different methods?

It is well-known that the D region strongly varies during sunrise and sunset. This was confirmed by the measurements carried out in August 2000, June 2001, and August 2015. The time–height–intensity plot of the API scattered signal amplitude during the sunrise and sunset period is shown in Figure 11. It is clear that in the D region, a decrease in the signal amplitude occurs upon the variation of the solar zenith angle from 90° to 105°. An increase in the scattered signal occurs upon decreasing the solar zenith angle from 97° to 90°. This is accompanied by a clear sunrise–sunset asymmetry, which manifests itself in the fact that at sunset, the scattered signals have a larger amplitude and occupy a larger altitude interval than at sunrise. During sunset, weak signals from the upper D region are seen for about an hour after the region is fully shadowed (i.e., after sunset at these heights). The wider and deeper amplitude minimum formed between the D and E layers during sunrise is clearly visible. These processes are well-described by a model involving a single negative-ion species O_2^- Such a model allows one to obtain variations in the number density of atomic oxygen and excited oxygen molecules in the $^1\Delta_g$ state and shows a significant increase in the atomic-oxygen density during sunrise [21,44].

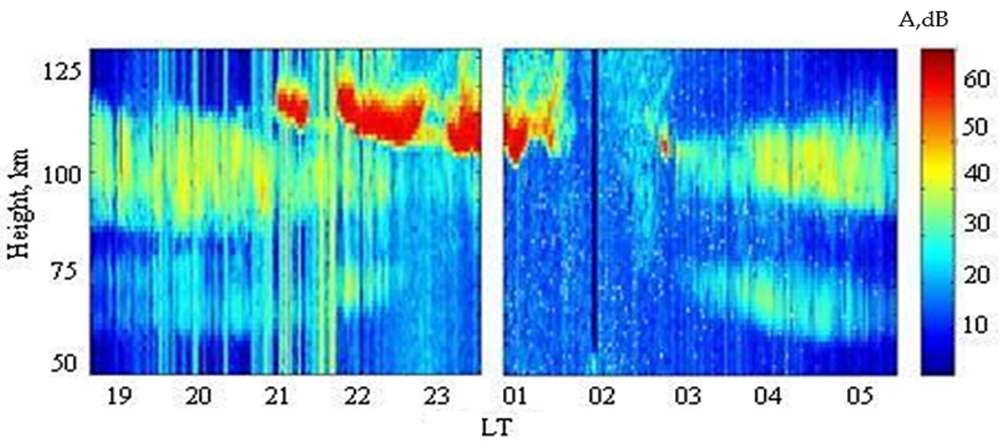

Figure 11. Height–time–intensity plot of API scattered signal amplitude A in sunset–sunrise period on 15–16 June 2001. Stratification of the D region is clearly visible before sunset from 19 to 21 LT. The lower boundary of the wave-like modulated sporadic E layer descended from 113 to 99 km. From [19,44].

Modeling performed in [21,44] showed that a sharp decrease in τ at altitudes above 75 km is due to an increase in the concentration of atomic oxygen, which leads to an increase in the rate of detachment of electrons from negative ions and a corresponding decrease in the relaxation time. At the same time, there is a sharp drop in the concentration of negative ions, and, in fact, the API formation stops due to the attachment of electrons to oxygen molecules. Thus, from the height in the lower part of the D region, at which the amplitude of the API scattered signal begins to decrease and the API formation stops, one can estimate the height of the lower boundary of the range enriched of atomic oxygen. The lower boundary of the height at which atomic oxygen appears and the scattered signal disappears can be determined from the height profile of the relaxation time similar to those shown Figure 3c.

Figure 12 shows the temporal variation of the height h_1 in the mesosphere, at which the amplitude of the scattered signal began to sharply decrease (black dots) and the height h_2 at which the scattered signal completely disappears (red dots). According to [11,21], the height h_1 can be considered as the height of the lower boundary of the region enriched in atomic oxygen. One can see that most of the h_1 values there are at 74, 76, and 77 km. The altitude at which the scattered signal completely disappears mainly varies within the range of 79–82 km. The API scattered signal usually reappears at an altitude of 90 km, when irregularities are formed due to plasma redistribution.

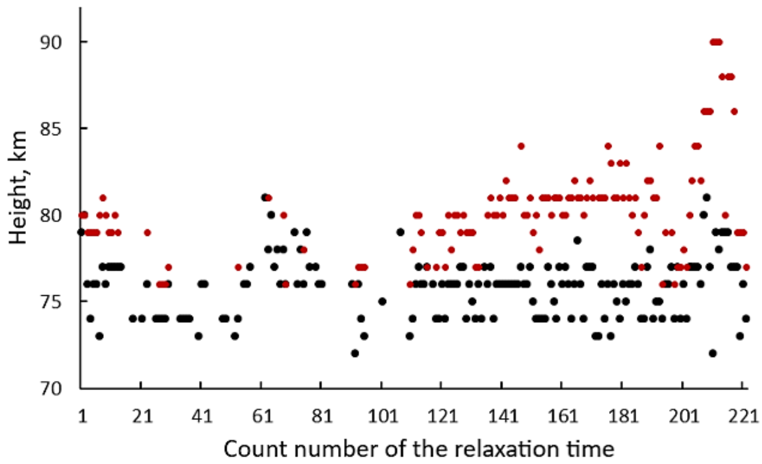

Figure 12. API relaxation time 11 September 2019. Black line is the height h_1 of the lower boundary of atomic oxygen; the red one is the height h_2 of the resumption of the scattered signal. From [45].

3.4. Plasma Vertical Velocity

Vertical movements are part of the general atmospheric circulation. This type of movement is still the least studied to date. At altitudes of 50–120 km, plasma is a passive admixture and is entrained by the motion of neutral gas; in this case, the velocity of the vertical motion of the plasma is equal to the velocity of the neutral medium [46]. The vertical plasma velocity V is determined by measuring the phase φ of the scattered signal as $V = \frac{\lambda}{4\pi}\frac{d\varphi}{dt} = \frac{c}{4\pi f n}\frac{d\varphi}{dt}$, where f is the frequency of high-power and probe radio waves, n is the refractive index, and c is the light velocity in vacuum. The formula determines the plasma vertical velocity, which coincides with the neutral component velocity for heights up to 120 km. Negative values denote the ascent.

Estimation of the possible systematic error in determining the vertical velocity V is substantiated in [11]. For the extraordinary component of the probe wave under ordinary ionospheric conditions, it does not exceed $\Delta V \approx 0.05$ m/s. The seasonal-daily variations of the vertical velocity were studied in experiments in 1990–1992. The seasonal variation of the average daily and monthly average V values was obtained at altitudes of 97–117 km. The nature of seasonal-daily variations in velocity was revealed to be complex: upward movements dominated above 90 km (up to 70% of all data). The average monthly velocity values were about 1 m/s at altitudes below 100 km, increasing to 5 m/s with increasing altitude. The results of the study of vertical movements in different environmental conditions are also contained in [38,47–53].

Figure 13 shows the height-temporal dependence of the vertical velocity averaged over 5 min on 13 August 2015.

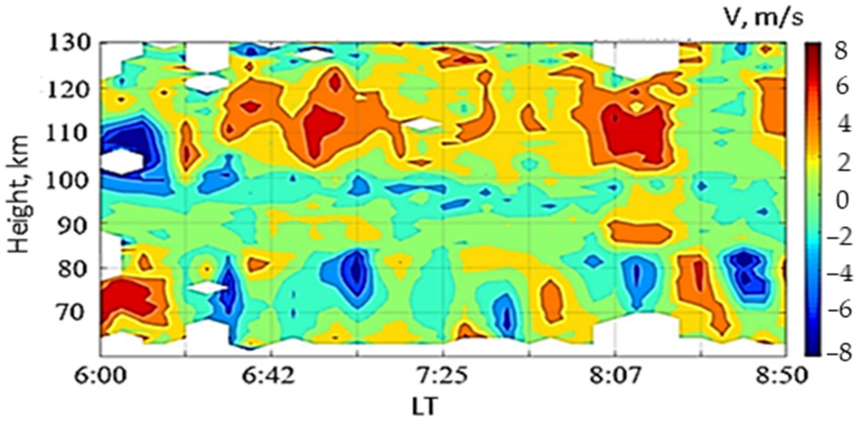

Figure 13. Vertical plasma velocity is equal to velocity of the neutral component on 13 August 2015 from 06:00 to 08:50 LT. You can see the change in the direction and magnitude of the vertical velocity in height and time. From [53].

The manifestation of atmospheric waves in vertical velocity variations is shown in Figure 14 in the temporal dependence of the velocity of vertical motion at an altitude of 100 km (a) and 105 km (b) during observations on 25 October 2018.

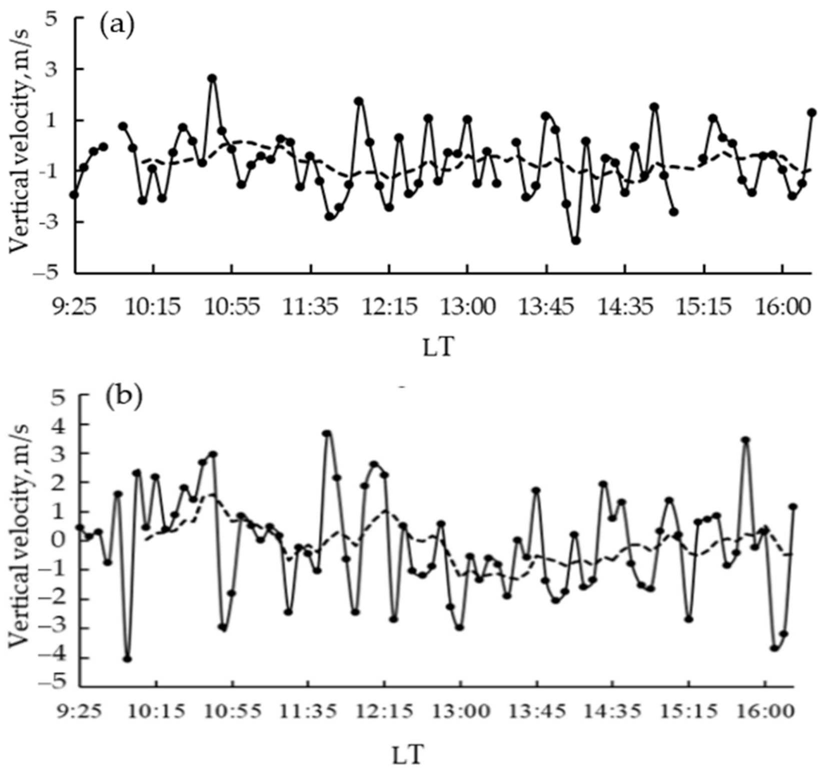

Figure 14. Temporal dependence of the velocity of vertical motion at an altitude of 100 km (**a**) and 105 km (**b**) during observations on 25 October 2018. Each point on the graphs was obtained via averaging velocity values over 5 min. Dashed curve was obtained with the running-average method over an interval of 40 min (eight points) in order to smooth out fluctuations of smaller periods.

The main features of the vertical velocity are fast temporal variations and the change in the magnitude and direction of the velocity within 15 s, that is, during one measurement. The value can reach up to 10 m/s or more. There is a change in the magnitude and direction of the velocity with height, and wave-like temporal variations are noted. In this case, the average values of the vertical velocity over long time intervals are mainly a few meters per second. The large velocity values compared with the models of atmospheric circulation indicate a significant influence of atmospheric waves. The height and temporal variation of the vertical velocity often have a wave-like appearance and occur with a periodicity characteristic of internal gravity waves. The most pronounced periods are 5–15, 30, 45, and 60 min. During long-term measurements for many hours, velocity variations were observed with a period of up to 4–5 h with a characteristic vertical scale of variations of 5–15 km.

The effect of vertical velocity variations on the formation of the sporadic layer E was studied in [19,30,36,38,39]. Figure 15 shows an example of the registration of the sporadic layer E on the ionogram (a), the height dependence of the scattered signal amplitude (b), and the vertical velocity profile (c) with a change in the direction at a height of 100 km.

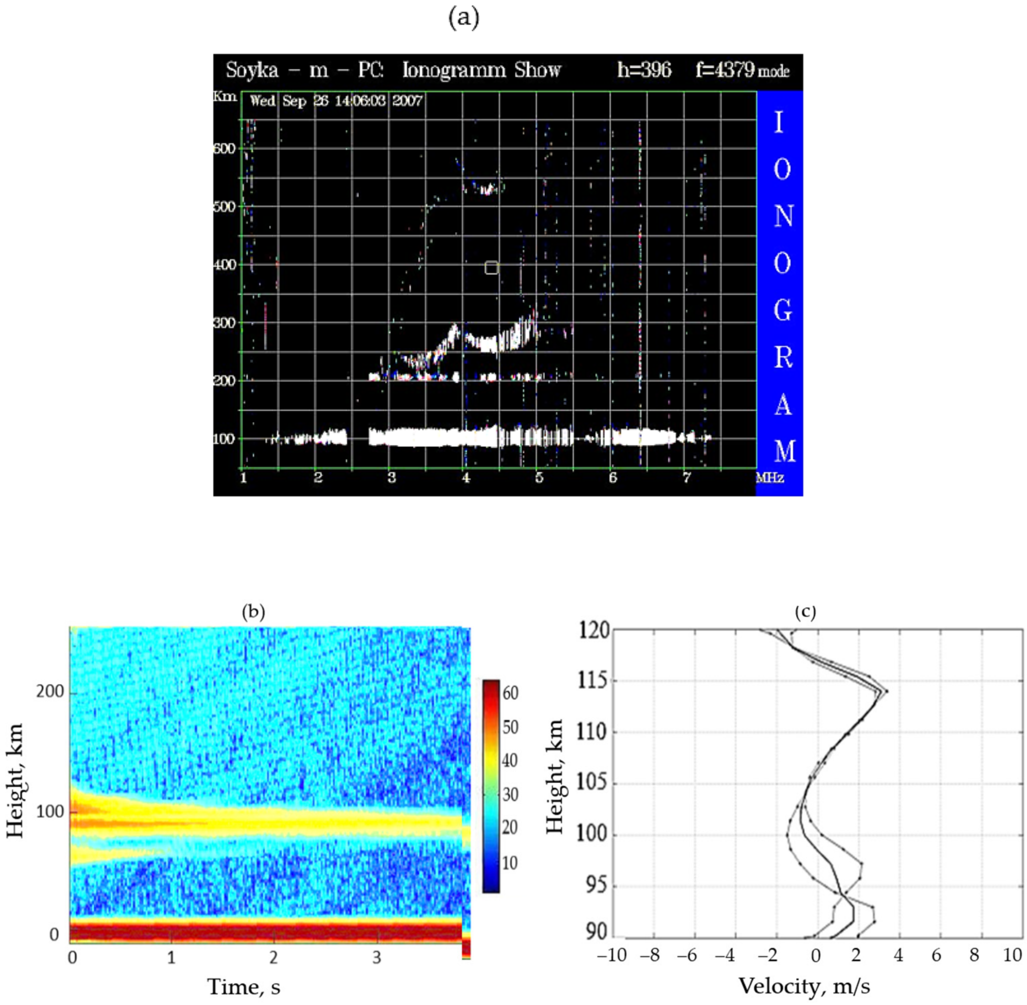

Figure 15. Example of registration of sporadic layer E on ionogram (**a**), height dependence of the scattered signal amplitude (**b**), and vertical velocity profile with a change in direction at a height of 100 km (**c**).

In many sessions, the change in the direction of the vertical velocity took place at the height of the layer formation, and the magnitude of its vertical gradient was sufficient for the formation of mid-latitude sporadic E_s layers, which were observed in experiments at the SURA heating facility. The height gradient of the vertical velocity determined from the results of measurements with a value of the order of 10^{-4} s^{-1} is sufficient for the shearing of metal ions into a sporadic layer formed at a height where the velocity becomes equal to zero.

4. API Technique and the Neutral Atmosphere

The determination of the temperature and density of the neutral component at altitudes of 90–130 km is based on the diffusion dependence of the scattered signal relaxation time given in Section 3.2. The basis for the determination of the parameters of the neutral atmosphere is the experimentally obtained altitudinal dependence of the relaxation time τ(h) of a signal scattered by periodic inhomogeneities [11,18]. The results of the determination of the temperature under different ionospheric conditions were given in [11,18,22,23,40,48–51,54,55].

4.1. Temperature and Density in the E Region

The method for determining the neutral temperature and density is described in detail in [11,18]. In the absence of the sporadic E layer and turbulence, the height dependence of the API relaxation time $\tau(h)$ is nearly exponential. The frequency ν_{im} of collisions of ions with neutral species is proportional to the density of the atmosphere ρ, and the background temperatures of ions T_i and electrons T_e are equal to the neutral temperature T at these heights. By measuring the altitude dependence τ(h) and assuming that $T \approx$ const within a small height interval, the temperature and density of the neutral atmosphere are given by the formulas $T = \frac{MgH}{\kappa}$, $\rho = \frac{8K^2\kappa T\tau}{\beta}\frac{M}{M_i}$, where H is the atmosphere height scale, determined from the τ(h) dependence; and M_i and M are the mean masses of the ions and neutral molecules, respectively; with the proportionality factor set equal to $\beta \approx 0.38 \times 10^{-10}$ cm^3/s. Estimates showed that the error of temperature and density measurements did not exceed 10% and 15%, respectively.

In [11,18,22,23,40,55–57], the features of temperature and density variations obtained by this method were studied. They contain many examples and discussions of the features of height profiles and temporal variations of these parameters. The temperature of the neutral atmosphere at altitudes of 90–130 km varied, as a rule, in the range of 100–250 K, and the temporal temperature and density variations from 5 min to several hours were observed.

Figure 16 shows the temporal variations of the neutral temperature (points) and vertical velocity (circles) at heights of 100 (a) and 110 km (b) on 26 September 2016, and the temperature (points) and density (circles) of the neutral component at an altitude of 105 km after sunrise on 13 June 2015, averaged over a 5-min interval (c). Another example of the neutral temperature and density variations at a height 100 km on 26 September 2016 and 28 September 2017 is shown in Figure 17. One can see a strong variability of the atmosphere parameter. It agrees with the measurements of these parameters by other methods [40].

Figure 18 shows the height profiles of the temperature in several sessions on 4 April 2006. On the left panel, typical smooth profiles with a minimum at a height of ~106 to 108 km are shown. This type of profile can be caused by the propagation of atmospheric waves [52]. These profiles are characterized by a large temperature gradient of about $dT/dz \approx -$(17–20) K/km in their lower part.

Based on the analysis of such profiles, an assumption about the development of instabilities in such an environment was made [52]. These instabilities should have led to a distortion of the smooth profile. On the basis of the analysis of such profiles, several instances of the development of instabilities were directly revealed in the scattering volume. Examples of such temperature profiles are shown on the right panel of Figure 18.

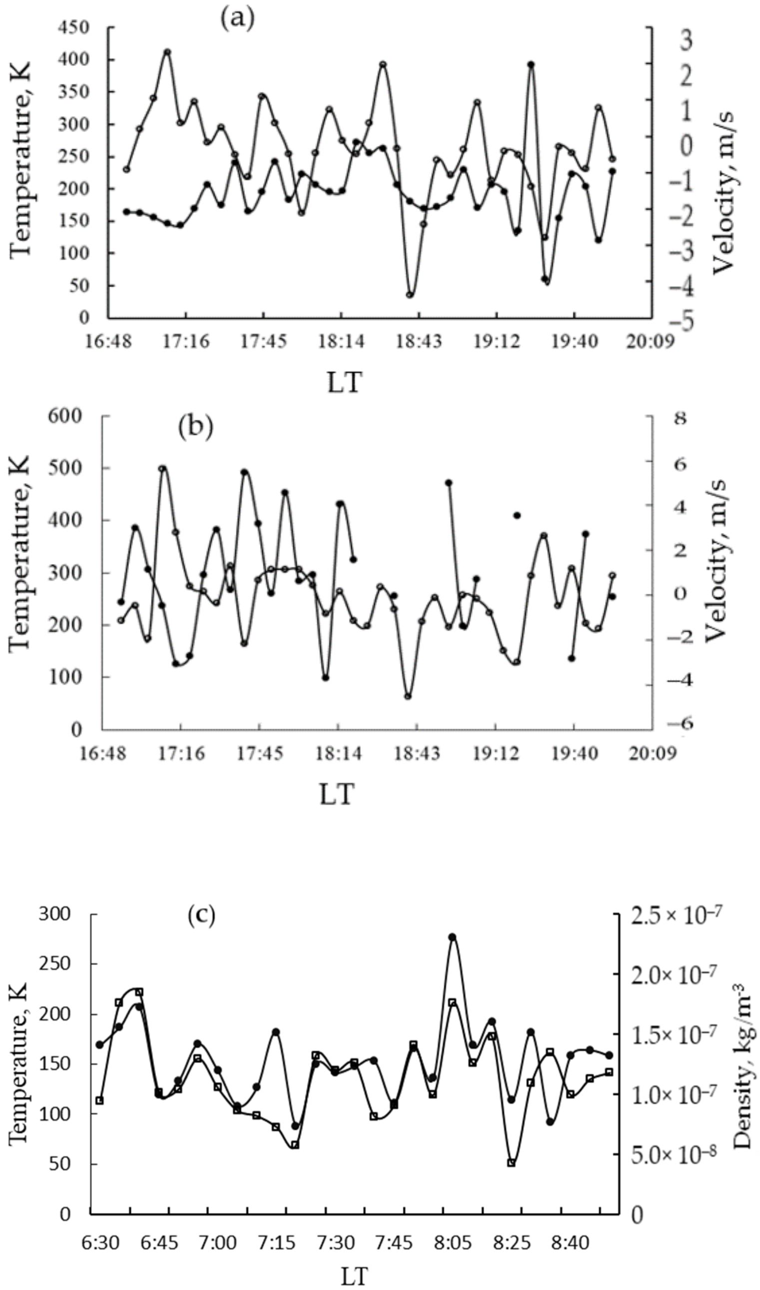

Figure 16. Temperature (points) and vertical velocity (circles) at height 100 (**a**) and 110 km (**b**) on 26 September 2016; temperature (points) and density (circles) of the neutral component at an altitude of 105 km after sunrise on 13 June 2015, averaged over a 5-min interval (**c**).

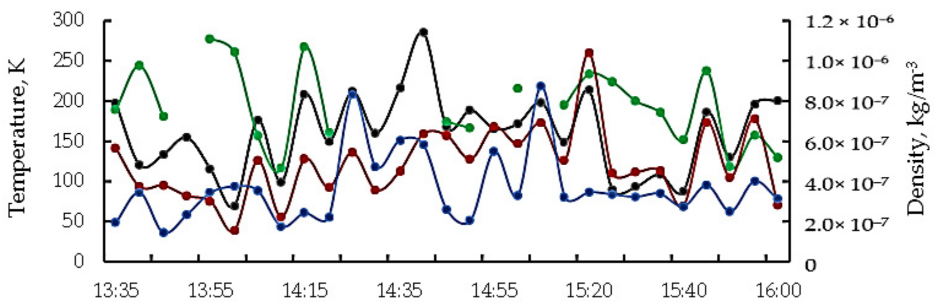

Figure 17. Neutral temperature and density at height 100 km on 26 September 2016 (green and blue points, respectively) and 28 September 2017 (black and red, respectively). From [53].

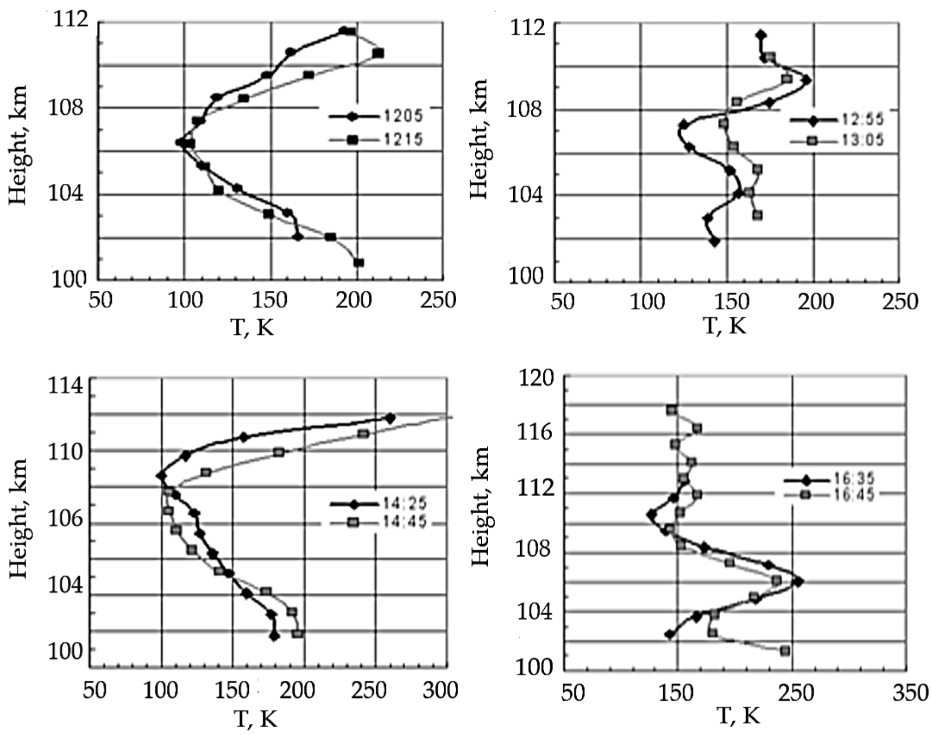

Figure 18. Examples of height profiles of neutral temperature in several sessions on 4 April 2006. Typical smooth profiles with minimum at the height of ~106 to 108 km (left panel) and gradients $dT/dz \approx -(17\text{–}20)\ K/km$ in their lower part; typical «disturbed» $T(h)$-profiles. From [52].

4.2. Turbulent Velocity and Turbopause Level

The mesosphere and low thermosphere are regions of developed dynamics caused by the propagation of atmospheric waves, turbulence, and winds. The height-temporal dependences of the API relaxation time are used to determine a large number of characteristics of the ionosphere and neutral atmosphere [11], including some parameters of the neutral turbulence. Turbulent motions of the medium destroy the artificially created periodic structure. The effect of turbulence manifests itself through a decrease in the amplitude and relaxation of the API scattered signal. For example, as demonstrated in Figure 19a, the diffusion law of relaxation corresponds to the altitude range of 100–125 km. The values of relaxation times are in good agreement with the diffusion dependence. Below 100 km, atmospheric turbulence begins to have an effect, and the relaxation time of the scattered signal decreases as compared with the diffusion time. A decrease in the relaxation time relative to the diffusion spreading time of inhomogeneities makes it possible to determine the turbulent velocity up to the height of the turbopause, near of which the turbulent velocity approaches zero. This is the level at which turbulent mixing of atmosphere gases is replaced by their diffusion separation. In [11], the problem of the influence of atmospheric turbulence on the amplitude and relaxation time of the scattered signal was considered in detail, taking into account the velocity field distributed according to a certain law (several distributions were considered). Assuming that the distortions of the periodic structure are created only by the field of vertical velocities, and the scattering volume is much greater than the API height scale $\Lambda = \lambda/2$, the expression for the turbulent velocity V_t is obtained in the form $V_t = \left(\sqrt{2}K\tau_t\right)^{-1} = \frac{\left(\tau_t^{-1} - \tau_d^{-1}\right)}{\sqrt{2}K}$, where τ_d is the diffusional relaxation time caused by ambipolar diffusion, and τ_t is the turbulent one.

The results of the determination of the turbulent velocity for 3 days of observations are accumulated in Figure 19b–d namely, from 12:10 to 17:10 LT on 11 September 2019, from 18:05 to 19:10 on 12 August 2015, and from 12:45 to 15:45 on 28 September 2018. As a rule, each point was obtained via averaging the relaxation time of the scattered signal over a time interval of 5 min.

Let us note some features of the altitude–time variations of the turbulent velocity. First is the variability of speed over time, which in Figure 18 appears as a spread of its values at each height. The maximum scatter of the turbulent velocity was about ΔV_t = 5 m/s at an altitude of 95 km for observations on 12 August 2015. The maximum velocity at this altitude was 6 m/s. In observations on 11 September 2019 and 28 September 2018, the maximum scatter ΔV_t ranged from 1.5 m/s to 2.2 m/s at heights of 90–93 km. The maximum values of V_t = 2.2–4.5 m/s were obtained at heights of 82–85 km, i.e., at mesopause heights. In general, the determination of the turbulent motion velocity from measurements of the characteristics of signals scattered by artificial periodic inhomogeneities showed that turbulent motions, along with regular vertical transport, make a large contribution to the dynamics of the lower.

The decrease in the amplitude of the scattered signal under the influence of the atmospheric turbulence begins at the turbopause level. Figure 20 shows a typical example of the temporal variations of the turbopause level.

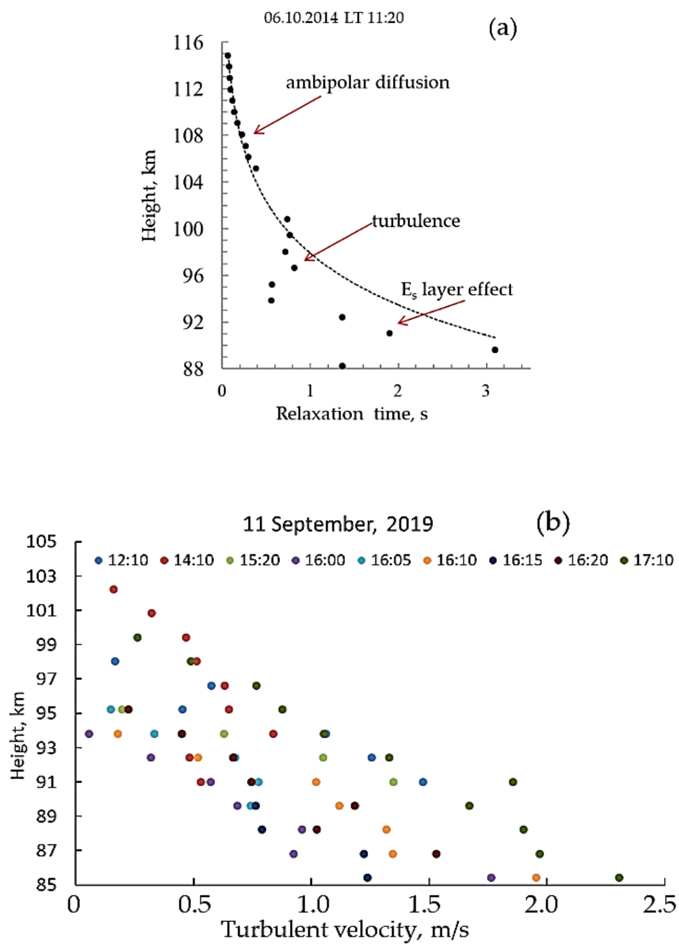

Figure 19. *Cont.*

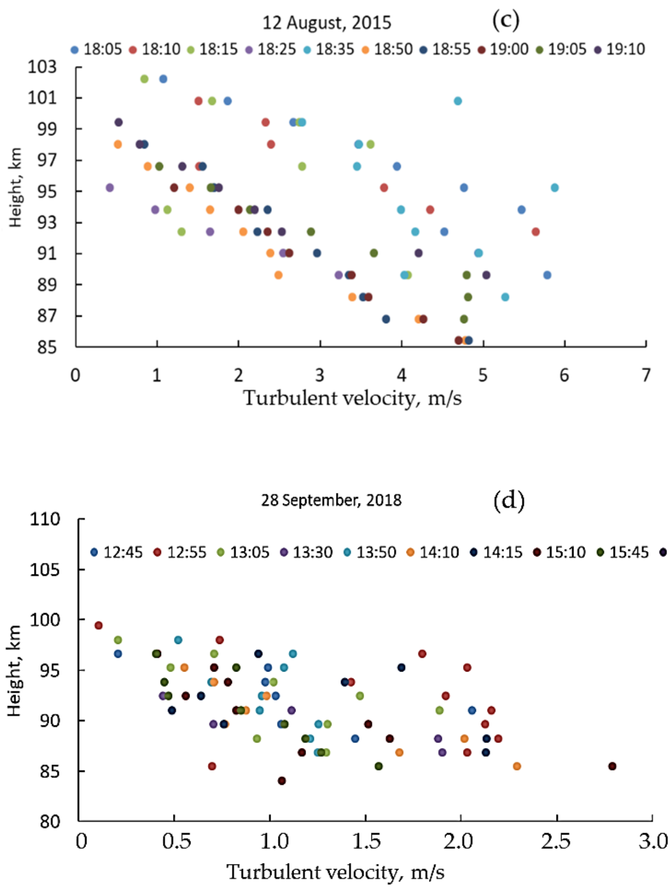

Figure 19. (**a**) The diffusion law of relaxation corresponds to the altitude range of 100–125 km; Dependences of turbulent velocities on altitude for 3 days of observations on (**b**) 11 September 2019, (**c**) 12 August 2015, and (**d**) 28 September 2018 at altitudes below the turbopause level. Dots of different colors refer to different measurement sessions. The figure shows the turbulent velocity can reach 2–3 m/s, increasing at certain times up to 5–7 m/s, that is, a value close to the regular vertical velocity of the environment. From [54].

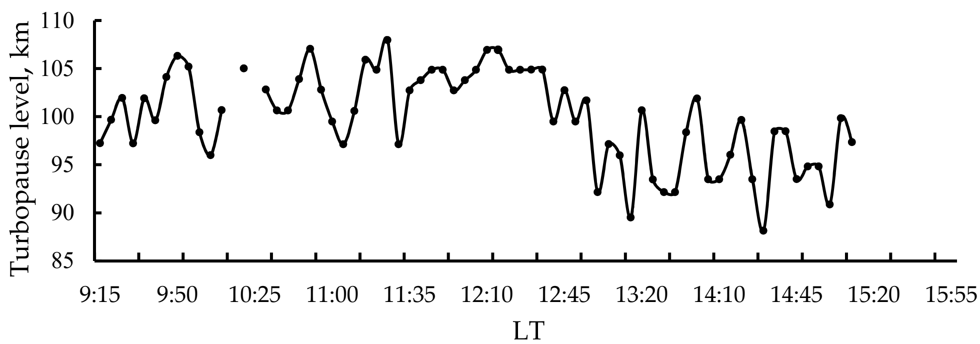

Figure 20. Variations of turbopause level on 26 October 2018 and its wave-like oscillation. Each point on the figure was obtained from the relaxation time values averaged over 2 min intervals. The variability in the turbopause level over time and the wave-like nature of variations is a common feature in the turbopause level on this day and others. From [54].

Tolmacheva et al. [40] presented and discussed the first results of the determination of the turbopause level based on the study of the ionosphere by the API technique in 2007–2014. A detailed analysis of the altitude profiles of the relaxation time obtained in these experiments showed that the minimum possible altitude to determine the parameters of the neutral atmosphere (temperature and density) with this method can be considered a marker of the turbopause level. According to the observational data given in [40], it was concluded that the average level of the turbopause was 99–102 km in the autumn season. In the evening hours, this border tended to decrease to 94 km. The turbopause level generally varied in an altitude range of 94–106 km. Its variations often had a wave-like component with periods from 10–15 to 30–40 min. It was also concluded that the region with turbulence can extend to 110 km under conditions of developed convective instability, with a significant increase in temperature. These conclusions are generally confirmed by the results of later experiments performed at the SURA facility in 2015–2019 [54,55].

5. Study of Natural Phenomena Using the API Technique

API observations during sunset and sunrise hours and during solar eclipses provide important information on the state of the ionosphere and neutral atmosphere [11,19,44]. The API technique allows us to study the features of the twilight and night ionosphere and the ionosphere during the solar eclipses.

5.1. Sunset–Sunrise Phenomena

Sunset–sunrise phenomena in the D region were studied in detail in [19]. In Section 3, the result of one of the first sunset–sunrise observations, which were carried out in the evening, night, and morning on 15–16 June 2001, is discussed. Figure 11 shows an example of the record by the API scattered of the night E_s layer descending from the altitude of 120–125 km to the altitude of 105–110 km with a velocity of 1 m/s. The time–height–intensity plot shows the API scattered signals in the D region (60–85 km) and in the E layer (90–120 km). The wave-like modulation of the E_s layer with periods from 15 min to 30 and 60 min is clearly visible [19].

Similar data were obtained on 12–13 August 2015. The height–time–amplitude and height–time–vertical velocity plots are shown in Figure 21a,b. Negative values of the vertical velocity denote the ascent. The figure shows scattered signals in the D region at a height of 70–85 km that appear at high altitudes with approaching sunset, signals from the E region at 90–130 km, and signals from the sporadic layer E. The layer E_s at sunset descended similarly to that shown in Figure 11. At dawn, the sporadic layer appeared at an altitude of 100 km and existed until the end of the observations. The vertical velocity constantly changed its direction, which was noticeably different for the morning and sunrise hours. The time dependences of the neutral temperature and vertical velocity were obtained from the data of measurements at sunrise. Their deep variations noted with a period of 15 to 90 min were presented in [18].

During the hours of transition from light to shadow (this also applies to an eclipse), wave-like perturbations with periods from 15 to 90 min appeared in the variations of many measured parameters. In the altitude profiles of temperature and velocity (here not given), a complex character of changes with local temperature minima and maxima is observed, which may be caused by the development of hydrodynamic instabilities of the environment or atmospheric wave propagation [52].

Many studies considered the interaction of regions E and F during the propagation of medium-scale traveling ionospheric disturbances (TIDs), as well as the influence of solar thermal tidal motions that cause the appearance of the so-called descending intermediate E_s layers [31–33]. A feature of the intermediate E_s layers is the appearance at heights between the E and F regions and a further downward movement toward the E region.

We note that, at night, the regular E and, moreover, D regions are not detected by backscattering radars since the background ionization drops by two orders of magnitude, while the API method makes it possible to study the lower ionosphere with very small t electron density values.

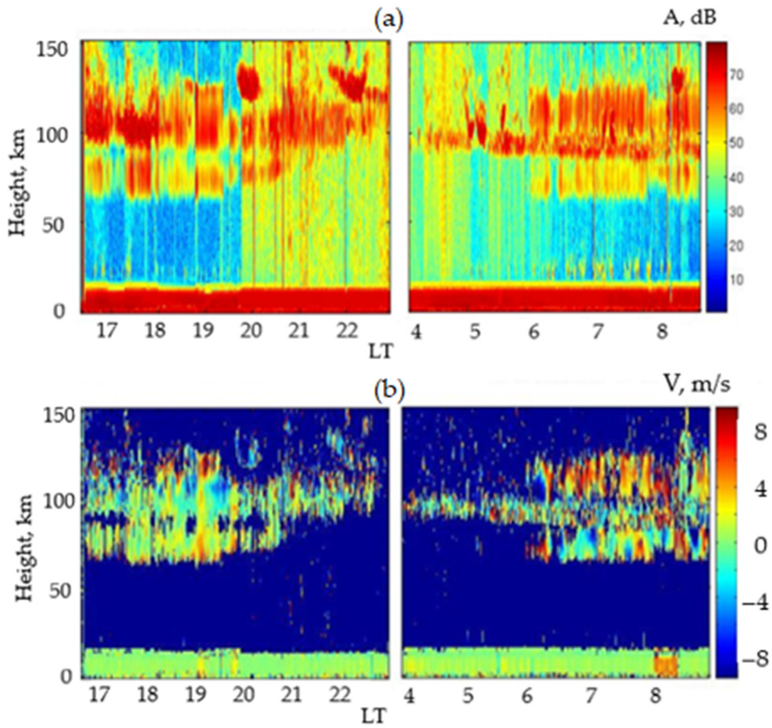

Figure 21. Time–height dependence of the API scattered signal amplitude A (**a**) and vertical plasma velocity (**b**) in sunset–sunrise period on 12–13 August 2015.

5.2. Solar Eclipse

Based on the measurements of the characteristics of the signal scattered by the API during the partial solar eclipses on 11 August 1999, 1 August 2008, and 20 March 2015, the response of the lower ionosphere to the solar eclipse was studied, including variations in the electron concentration, temperature, and neutral component density, as well as the velocity of vertical and turbulent motions [56,57]. Figure 22 shows a time–height–intensity plot of the amplitude of the API scattered signal (a) and vertical plasma velocity (b) during the partial solar eclipse of 20 March 2015.

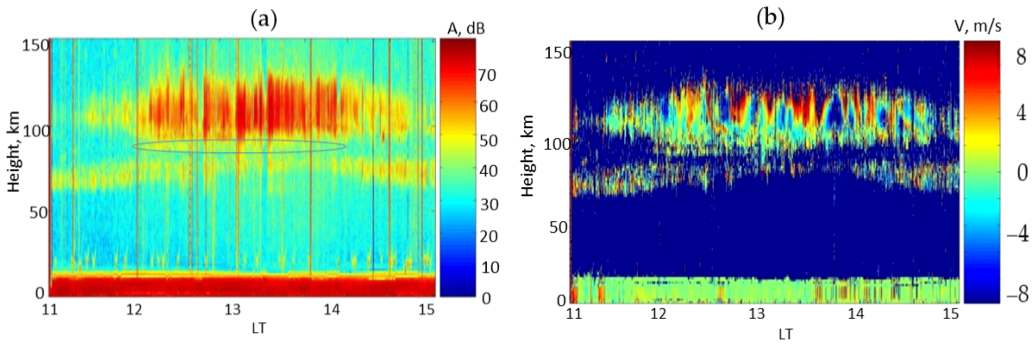

Figure 22. Time–height–intensity plot of the amplitude of the API scattered signal (**a**) and vertical plasma velocity (**b**) during partial solar eclipse of 20 March 2015 with a phase at observation point of 0.586. The oval (**a**) shows the "mesospheric" signal from altitudes of 84–88 km, which appeared shortly before the beginning of the eclipse and disappeared after it ended. This unusual signal relaxed very slowly over 2–4 s. Its nature is still unclear. From [56].

Figure 22 shows the dependences of the amplitude of the API scattered signal (a) and the vertical plasma velocity before, during, and after the end of the eclipse at the heights of the mesosphere and lower thermosphere. Scattered signals are clearly visible in the D region (at heights 65–86 km), E region (90–130 km), and sporadic E layer (100–115 km), which was also registered by CADI ionosonde. Let us briefly note the main features of

API scattered signals observed during the solar eclipse. The amplitude of the scattered signal significantly increased during the eclipse, especially in the E region (by 30–40 dB). The most probable reason for this is a decrease in absorption due to a general decrease in the electron concentration with a decrease in the Sun ionizing radiation. Scattered signals began to occupy an increasing range of heights in the E region during the eclipse. The scattered signals in the D region were more intense than the API signals scattered in the E region. This is a somewhat unusual phenomenon. Figure 22 shows an increase in the height of the scattered signal, that is, an increase in the height of the API formation in the D region, which is similar to the transition to the night mode of the ionosphere [20]. Near the maximum phase of the eclipse, a layering of the D region was observed, as was observed during sunset and sunrise [45,56,57]. The oval in the figure shows an unusual signal at altitudes of 84–88 km similar to the summer mesospheric echo.

During the eclipses, the intensity of the turbulence of the lower ionosphere increased, with values of the turbulent velocity V_t rising up to 7 m/s, the amplitudes of the signals backscattered by the artificial periodic irregularities in the E layer also increased, the D layer showed stratification, and signals scattered from the mesopause emerged. Wave motions with IGW periods manifested themselves in the temporal variations of the characteristics of the scattered signals, as well as of the temperature, density, and vertical velocity. During a solar eclipse, the Earth's ionosphere approaches its nighttime state, so the time variations of the characteristics of its ionized and neutral components in sunset and sunrise hours and during solar eclipses are similar in many respects.

5.3. Atmospheric Waves

It is well-known that the region of the mesosphere and lower thermosphere is characterized by many dynamic phenomena, including the propagation of atmospheric waves [58–61]. Some results of the measurements of the ionosphere and neutral atmosphere parameters such as the electron density, velocity of the vertical plasma motion and turbulent velocity, neutral atmosphere temperature, and density by the API technique and their examples presented in previous sections of the article showed that the temporal variations of the parameters are mostly caused by wave processes including IGWs or TIDs. Many examples of variations in measured parameters can be found in [11] and are cited above. The spectral analysis has shown that temporal variations of the parameters contain oscillations with period from minutes to some hours. On various conditions, periods with durations of 5–10, 15, 20, 30–40, and 60 min were observed. Furthermore, we have identified wave-like motions with periods of 1.5, 2.0, 2.5, 3.3, and 4.5 h. We tried to consider the effect of atmospheric waves on variations in ionospheric parameters at the heights of the mesosphere and lower thermosphere. In [37], the joint analysis of the variations of the plasma vertical velocity in neutral atmosphere temperature and density at a height of 80–110 km was performed based on the results of the API experiments in 1991–1992. About 30 sessions of duration from 1 to 6 h were selected. In these sessions, the oscillations amplitude made up an amount from 1.5 m/s to 4 m/s for vertical velocity and 6–20% for neutral temperature and density. The theoretical simulation of the IGW characteristics was carried out on the basis of the linear theory of their free propagation in an unbounded isothermal and undisturbed atmosphere. Based on the IGW polarization relations [62], we calculated the relative amplitudes of variations of the temperature and density with periods from 15 min to 4 h using the measured amplitudes of the vertical velocity [37]. Comparison of the modeling results with measured values showed their good agreement for waves with periods 15–30 min only. For periods longer than 100 min, there were no cases of reasonable agreement between the measured and simulated values. One can propose several explanations for the disagreement. Firstly, a quite crude model for free IGW propagation in an unbounded isothermal and undisturbed atmosphere has been used for simulation. Secondly, the linear theory of the IGW propagation may be inaccurate for disturbances of about 20–50% of the equilibrium ones. Thirdly, we did not take into account the possible superposition of waves from different sources and their nonlinear interaction. In addition, variations in atmospheric parameters are affected by the horizontal motions of the environment, which were also not taken into account.

Figures 9, 11, 13–16, 19 and 20 show that the altitude profiles of the electron density, vertical velocity of the plasma, and temperature and density of the neutral atmosphere at altitudes of 90–120 km are affected by atmospheric waves. Often, the perturbations of these parameters are unstable, which may be due to the propagation of IGWs and the evolution of instabilities of the environment. In [52], as applied to the results of measurements of atmospheric parameters by the API method, we analyzed hydrodynamic instabilities at altitudes of the mesosphere and lower thermosphere. In [52], the criteria for the development of hydrodynamic instabilities at these altitudes are given, and they are compared with the measurement results. It is concluded that the reason for the instability occurrence can be the negative temperature gradient. The criterion $dT/dh < -$(10–12) K/km is a sufficient condition for an instability evolution. When the criterion was fulfilled, the negative temperature gradient reaching $-20\ K/km$ and disturbances of atmospheric parameters manifested by deep height–temporal variations were recorded in the subsequent instants of time.

We studied the IGW propagation in the atmosphere with linear and heterogeneous height profiles of the neutral temperature as applied to the results of the diagnostics of the lower thermosphere [63–65]. It was shown that in the absence of regular wind in the environment, the IGW amplitude can increase, provided that the rate of temperature decrease with height exceeds the threshold level close to $-10\ K/km$. Based on our neutral temperature measurements, we concluded that polytropic IGW propagation with index of 2 is possible [66].

In concluding this section, we note that measurements of the characteristics of the atmosphere and ionosphere by the API method contributed to our studies of atmospheric waves.

6. Conclusions

The review is far from a complete illustration of the capabilities of the API method for studying the mesosphere and lower thermosphere. In general, the API technique provides a coverage of heights from the mesosphere to the height of reflection of a powerful wave in the F layer. The height resolution is about 1 km. The method has a high temporal resolution of the order of several seconds and can be used for a long time in any state of the ionosphere. Both fast and slow atmospheric processes and phenomena are available to the API technique. It is only important that the powerful wave, which creates inhomogeneities, be reflected from the ionosphere.

Long-term experiments on measuring important parameters such as the electron density, vertical plasma velocity, temperature, and density of the neutral component have shown a constant manifestation of atmospheric waves in their altitude–time variations. It was possible to determine the velocity of turbulent motion and the level of turbopause. It is shown that the vertical regular and turbulent velocities can be comparable in magnitude. A method was found to estimate the mass of the predominant metal ions in the sporadic E layer. In this review, we gave examples of studying twilight phenomena in the D and E regions and also demonstrated the effect of a solar eclipse on the characteristics of scattered signals.

These observations do not exhaust all the diagnostic possibilities of the API technique. Future studies may determine the electron density profile from the D region to the F2 layer by alternately creating and probing APIs at two slightly different frequencies. So far, insufficient attention has been paid to the experimental study of the processes of development of inhomogeneities. Finally, we attach great importance to the study and modeling of aeronomic processes in the D region.

Author Contributions: Conceptualization, N.V.B.; investigation, N.V.B. and G.I.G.; writing—original draft preparation, N.V.B.; writing—review and editing, N.V.B. and G.I.G.; supervision, N.V.B.; funding acquisition, N.V.B. and G.I.G. All authors have read and agreed to the published version of the manuscript.

Funding: This research was funded by the Russian Science Foundation under grant 20-17-00050.

Institutional Review Board Statement: Not applicable.

Informed Consent Statement: Not applicable.

Data Availability Statement: Not applicable.

Acknowledgments: The authors thank A.V. Tolmacheva, E.E. Kalinina, and I.N. Zhemyakov for research assistance. We thank the reviewers and the Editors for their productive and valuable comments.

Conflicts of Interest: The authors declare no conflict of interest.

References

1. Vilenskii, I.M.; Izraileva, N.I.; Kapel'zon, A.A.; Plotkin, V.V.; Freiman, M.E. *Artificial Quasi-Periodic Irregularities in the Lower Ionosphere*; Nauka: Novosibirsk, Russia, 1987; p. 188. (In Russian)
2. Belikovich, V.V.; Benediktov, E.A.; Getmantsev, G.G.; Ignat'ev, Y.A.; Komrakov, G.P. Scattering of radio waves from the artificially perturbed F region of the ionosphere (Engl. Translation). *JETP Lett.* **1975**, *22*, 243–244.
3. Fejer, I.A.; Djuth, F.T.; Gonzales, C.A. Bragg backscatter from plasma inhomogeneities due to a powerful ionospherically reflected radio waves. *J. Geophys. Res.* **1984**, *89*, 9145–9147. [CrossRef]
4. Djuth, F.T.; Groves, K.M.; Elder, J.H.; Shinn, E.R.; Quinn, J.M.; Villasenor, J.; Wong, A.Y. Measurements of artificial periodic inhomogeneities at HIPAS observatory. *J. Geophys. Res.* **1997**, *102*, 24023–24035. [CrossRef]
5. Rietveld, M.T.; Goncharov, N.P. Artificial periodic irregularities from the Tromso heating facility. *Adv. Space Res.* **1998**, *21*, 693–696. [CrossRef]
6. Rietveld, M.T.; Turunen, E.; Matveinen, H.; Goncharov, N.P.; Pollari, P. Artificial periodic irregularities in the auroral ionosphere. *Ann. Geophys.* **1996**, *14*, 1437–1453. [CrossRef]
7. Vierinen, J.; Kero, A.; Rietveld, M.T. High latitude artificial periodic irregularity observations with the upgraded EISCAT heating facility. *J. Atmos. Sol. Terr. Phys.* **2013**, *105–106*, 253–261. [CrossRef]
8. Hyssel, D.L.; McCarrick, M.J.; Fallen, C.T.; Vierinen, J. First artificial periodic inhomogeneity experiments at HAARP. *GRL.* **2015**, *42*, 1033–1297. [CrossRef]
9. Grach, S.M.; Sergeev, E.N.; Bakhmetieva, N.V.; Milikh, G.; Shindin, A.V. Preliminary results of the artificial periodic irregularities excited by the HAARP HF heater. In Proceedings of the 14th Ionospheric Effects Symposium (IES2015), Alexandria, VA, USA, 12–14 May 2015; Available online: http://ies2015.bc.edu/wp-content/uploads/2015/05/051-Grach-Paper.pdf (accessed on 15 July 2022).
10. Bakhmetieva, N.V.; Grach, S.M.; Sergeev, E.N.; Shindin, A.V.; Milikh, G.M.; Siefring, C.L.; Bernhardt, P.A.; McCarrick, M. Artificial periodic irregularities in the high-latitude ionosphere excited by the HAARP facility. *Radio Sci.* **2016**, *51*, 999–1009. [CrossRef]
11. Belikovich, V.V.; Benediktov, E.A.; Tolmacheva, A.V.; Bakhmet'eva, N.V. *Ionospheric Research by Means of Artificial Periodic Irregularities*; Copernicus GmbH: Katlenburg-Lindau, Germany, 2002; p. 160.
12. Belikovich, V.V.; Benediktov, E.A. Investigation of the lower D-region of the ionosphere using artificial periodic irregularities. *Radiofizika* **1986**, *29*, 1283–1296. (In Russian)
13. Belikovich, V.V.; Benediktov, E.A.; Terina, G.I. Diagnostics of the lower ionosphere by the method of resonance scattering of radio waves. *J. Atmos. Terr. Phys.* **1986**, *48*, 1247–1253. [CrossRef]
14. Bakhmet'eva, N.V.; Belikovich, V.V.; Benediktov, E.A.; Vyakhirev, V.D.; Goncharov, N.P.; Tolmacheva, A.V.; Korotina, G.S. Studies of the ionosphere and neutral atmosphere using artificial periodic inhomogeneities in the ionospheric plasma. *Radio Sci.* **1998**, *33*, 583–594. [CrossRef]
15. Tolmacheva, A.V.; Bakhmet'eva, N.V.; Vyakhirev, V.D.; Bubukina, V.N.; Kalinina, E.E. Altitude–time variations in electron number density in the ionospheric E layer. *Radiophys. Quantum Electron.* **2011**, *54*, 365–375. [CrossRef]
16. Bakhmet'eva, N.V.; Belikovich, V.V.; Benediktov, E.A.; Bubukina, V.N.; Ignat'ev, Y.A. Investigation of wave motions in the lower ionosphere by the method of resonance scattering of radio waves from artificial periodic inhomogeneities. *Radiophys. Quantum Electron.* **1997**, *40*, 196–205. [CrossRef]
17. Belikovich, V.V.; Bakhmeteva, N.V.; Kalinina, E.E.; Tolmacheva, A.V. A New method for determination of the electron number density in the e region of the ionosphere from relaxation times of artificial periodic inhomogeneities. *Radiophys. Quantum Electron.* **2006**, *49*, 669–674. [CrossRef]
18. Belikovich, V.V.; Benediktov, E.A.; Goncharov, N.P.; Tolmacheva, A.V. Diagnostics of the ionosphere and neutral atmosphere at e-region heights using artificial periodic inhomogeneities. *J. Atmos. Sol.-Terr. Phys.* **1997**, *59*, 2447–2460. [CrossRef]

19. Bakhmet'eva, N.V.; Belikovich, V.V.; Kagan, L.M.; Ponyatov, A.A. Sunset–sunrise characteristics of sporadic layers of ionization in the lower ionosphere observed by the method of resonance scattering of radio waves from artificial periodic inhomogeneities of the ionospheric plasma. *Radiophys. Quantum Electron.* **2005**, *48*, 14–28. [CrossRef]
20. Bakhmet'eva, N.V.; Belikovich, V.V.; Benediktov, E.A.; Tolmacheva, A.V. Studies of the irregular structure of the ionosphere using scattering of radio waves on artificial periodic inhomogeneities. *Radiophys. Quantum Electron.* **2001**, *44*, 924–934. [CrossRef]
21. Belikovich, V.V.; Benediktov, E.A.; Trunov, D.V. Height profiles of the amplitude and relaxation time of artificial periodic irregularities in the D-region. *Geomagn. Aeron.* **2000**, *40*, 733–738.
22. Benediktov, E.A.; Belikovich, V.V.; Tolmacheva, A.K. Some results of measurement of atmospheric temperature and density using artificial periodic inhomogeneities of the ionospheric plasma. *Radiophys. Quantum Electron.* **1998**, *41*, 229–235. [CrossRef]
23. Tolmacheva, A.V.; Belikovich, V.V. Measurements of the temperature and density of the upper atmosphere using artificial periodic irregularities during the summer seasons of 1999–2002. Int. *J. Geomagn. Aeron.* **2004**, *5*, GI1008. [CrossRef]
24. Belikovich, V.V.; Benediktov, E.A.; Bubukina, V.N.; Vyakhirev, V.D. Artificial periodic inhomogeneities and a model for the lower part of the D region. *Radiophys. Quantum Electron.* **1999**, *42*, 431–437. [CrossRef]
25. Bakhmet'eva, N.V.; Belikovich, V.V.; Ponyatov, A.A.; Tolmacheva, A.V.; Kagan, L.M.; Kelley, M.C.; Nicolls, M.J. New results of studying the lower ionosphere by the method of resonance scattering of radio waves from artificial periodic inhomogeneities. *Radiophys. Quantum Electron.* **2005**, *48*, 673–685. [CrossRef]
26. Tolmacheva, A.V. Results of the ion–neutral collision frequency measurements in the lower thermosphere by the method of resonance scattering of the radio waves by artificial periodic irregularities. *Radiophys. Quantum Electron.* **2015**, *58*, 245–251. [CrossRef]
27. Frolov, V.L.; Bakhmet'eva, N.V.; Belikovich, V.V.; Vertogradov, G.G.; Vertogradov, V.G.; Komrakov, G.P.; Kotik, D.S.; Mityakov, N.A.; Polyakov, S.V.; Rapoport, V.O.; et al. Modification of the Earth's ionosphere by high power high frequency radio waves. *Phys.-Uspekhi* **2007**, *50*, 315–324. [CrossRef]
28. Belikovich, V.V.; Bakhmet'eva, N.V.; Bubukina, V.N.; Vyakhirev, V.D.; Kalinina, E.E.; Komrakov, G.P.; Tolmacheva, A.V. Results of determining the electron number density in the ionospheric E region from relaxation times of artificial periodic irregularities of different scales. *Radiophys. Quantum Electron.* **2008**, *51*, 431–437. [CrossRef]
29. Bakhmetieva, N.V.; Grigor'ev, G.I.; Tolmacheva, A.V.; Kalinina, E.E. Atmospheric turbulence and internal gravity waves examined by the method of artificial periodic irregularities. Russ. *J. Phys. Chem. B* **2018**, *12*, 510–521.
30. Yusupov, K.M.; Bakhmetieva, N.V. Sporadic E layer with a structure of double cusp in the vertical sounding ionogram. *Atmosphere* **2021**, *12*, 1093. [CrossRef]
31. Wilkinson, P.J.; Szuszczewicz, E.P.; Roble, R.G. Measurements and modeling of intermediate, descending, and sporadic layers in the lower ionosphere: Results and implications for global-scale ionospheric-thermospheric studies. *Geophys. Res. Lett.* **1992**, *19*, 95–98. [CrossRef]
32. Haldoupis, C.; Meek, C.; Christakis, N.; Pancheva, D.; Bourdillon, A. Ionogram height–time–intensity observations of descending sporadic E layers at mid-latitude. *J. Atmos. Sol.-Terr. Phys.* **2006**, *68*, 539–557. [CrossRef]
33. Mathews, J.D.; Bekeny, F.S. Upper atmospheric tides and the vertical motion of ionospheric sporadic layers at Arecibo. *J. Geophys. Res.* **1979**, *84*, 2743–2750. [CrossRef]
34. Shalimov, S.; Kozlovsky, A. High-latitude E and F region coupling signature: A case study results from rapid-run ionosonde. *J. Geophys. Res. Space Phys.* **2015**, *120*, 3033–3041. [CrossRef]
35. Yusupov, K.M.; Mathews, J.D.; Maruyama, T.; Akchurin, A.D.; Tolstikov, M.V.; Sherstyukov, O.N.; Filippova, E.A.; Safiullin, A.S. Amplitude variations of the reflected signal during vertical sounding of the ionosphere at middle latitudes. *Sol.-Terr. Phys.* **2020**, *6*, 72–80.
36. Bakhmetieva, N.V.; Belikovich, V.V. Results of studying the sporadic E layer by the method of resonant scattering of radio waves by artificial periodic inhomogeneities of the ionospheric plasma. *Radiophys. Quantum Electron.* **2008**, *51*, 862–873. [CrossRef]
37. Bakhmetieva, N.V.; Belikovich, V.V.; Grigor'ev, G.I.; Tolmacheva, A.V. Effect of acoustic gravity waves on variations in the lower-ionosphere parameters as observed using artificial periodic inhomogeneities. *Radiophys. Quantum Electron.* **2002**, *45*, 211–219. [CrossRef]
38. Bakhmet'eva, N.V.; Belikovich, V.V.; Ignat'ev, Y.A.; Ponyatov, A.A. Vertical motions in the lower ionosphere and a sporadic E layer. *Radiophys. Quantum Electron.* **1999**, *42*, 22–30. [CrossRef]
39. Bakhmet'eva, N.V.; Belikovich, V.V.; Egerev, M.N.; Tolmacheva, A.V. Artificial periodic irregularities, wave phenomena in the lower ionosphere and the sporadic E-layer. *Radiophys. Quantum Electron.* **2010**, *53*, 77–90. [CrossRef]
40. Tolmacheva, A.V.; Bakhmetieva, N.V.; Grigoriev, G.I.; Kalinina, E.E. The main results of the long-term measurements of the neutral atmosphere parameters by the artificial periodic irregularities techniques. *Adv. Space Res.* **2015**, *56*, 1185–1193. [CrossRef]
41. Bakhmet'eva, N.V.; Belikovich, V.V.; Benediktov, E.A.; Bubukina, V.N.; Goncharov, N.P.; Ignat'ev, Y.A. Investigation of acoustic gravity waves in the upper atmosphere by the artificial periodic inhomogeneities method at Nizhny Novgorod. *Radiophys. Quantum Electron.* **1996**, *39*, 224–228. [CrossRef]
42. Huuskonen, A.; Nygren, T.; Jalonen, L.L.; Bjorn, N.; Hansen, T.L.; Brekke, A. Ion composition in sporadic E layers measured by the EISCAT UHF radar. *J. Geophys. Res.* **1988**, *93*, 14603. [CrossRef]
43. Kopp, E. On the abundance of metal ions in the lower ionosphere. *J. Geophys. Res. Space Phys.* **1997**, *102*, 9967–9974. [CrossRef]

44. Belikovich, V.V.; Benediktov, E.A. Study of the twilight D-region of the Ionosphere using artificial periodic inhomogeneities. *Radiophys. Quantum Electron.* **2002**, *45*, 458–464. [CrossRef]
45. Bakhmetieva, N.V.; Kulikov, Y.Y.; Zhemyakov, I.N. Mesosphere Ozone and the lower Ionosphere under plasma disturbance by powerful high-frequency radio emission. *Atmosphere* **2020**, *11*, 1154. [CrossRef]
46. Gershman, B.N. *Dynamics of the Ionospheric Plasma*; Nauka: Moscow, Russia, 1974; p. 256. (In Russian)
47. Benediktov, E.A.; Belikovich, V.V.; Bakhmet'eva, N.V.; Tolmacheva, A.V. Artificial periodic inhomogeneities of the ionosperic plasma as a promising line in the ionospheric research. *Radiophys. Quantum Electron.* **2002**, *45*, 343–357. [CrossRef]
48. Benediktov, E.A.; Belikovich, V.V.; Bakhmet'eva, N.V.; Tolmacheva, A.V. Seasonal and daily variations of the velocity of vertical motions at altitudes of the mesosphere and lower thermosphere near Nizhny Novgorod. *Geomag. Aeron.* **1997**, *37*, 88.
49. Tolmacheva, A.V.; Grigoriev, G.I.; Bakhmetieva, N.V. The variations of the atmospherical parameters on measurements using the artificial periodic irregularities of plasma. *Russ. J. Phys. Chem. B* **2013**, *7*, 663–669. [CrossRef]
50. Bakhmetieva, N.V.; Grigoriev, G.I.; Tolmacheva, A.V.; Zhemyakov, I.N. Investigations of Atmospheric Waves in the Earth Lower Ionosphere by Means of the Method of the Creation of the Artificial Periodic Irregularities of the Ionospheric Plasma. *Atmosphere* **2019**, *10*, 450. [CrossRef]
51. Bakhmetieva, N.V.; Vyakhirev, V.D.; Grigoriev, G.I.; Egerev, M.N.; Kalinina, E.E.; Tolmacheva, A.V.; Zhemyakov, I.N.; Vinogradov, G.R.; Yusupov, K.M. Dynamics of the mesosphere and lower thermosphere based on results of observations on the SURA facility. *Geomag. Aeron.* **2020**, *60*, 96–111. [CrossRef]
52. Bakhmetieva, N.V.; Grigor'ev, G.I.; Tolmacheva, A.V. Artificial periodic irregularities, hydrodynamic instabilities, and dynamic processes in the mesosphere-lower thermosphere. Radiophys. *Quantum Electron.* **2011**, *53*, 623–637.
53. Bakhmetieva, N.V.; Zhemyakov, I.N. Vertical plasma motions in the dynamics of the mesosphere and lower thermosphere of the Earth. *Russ. J. Phys. Chem. B* **2022**, *16*. *in press*.
54. Bakhmetieva, N.V.; Grigoriev, G.I.; Vinogradov, G.R.; Zhemyakov, I.N.; Kalinina, E.E.; Pershin, A.V. Parameters of Atmospheric Turbulence and the Dynamics of the Lower Ionosphere in Studies at the SURA Facility. *Geomag. Aeron.* **2021**, *61*, 871–887. [CrossRef]
55. Tolmacheva, A.V.; Bakhmetieva, N.V.; Grigoriev, G.I.; Egerev, M.N. Turbopause range measured by the method of the artificial periodic irregularities. *Adv. Space Res.* **2019**, *64*, 1968–1974. [CrossRef]
56. Bakhmetieva, N.V.; Vyakhirev, V.D.; Kalinina, E.E.; Komrakov, G.P. Earth's lower ionosphere during partial solar eclipses according to observations near Nizhny Novgorod. *Geomagn. Aeron.* **2017**, *57*, 58–71. [CrossRef]
57. Bakhmetieva, N.V.; Bubukina, V.N.; Vyakhirev, V.D.; Kalinina, E.E.; Komrakov, G.P. Response of the lower ionosphere to the partial solar eclipses of 1 August 2008 and 20 March 2015 based on observations of radio-wave scattering by the ionospheric plasma irregularities. *Radiophys. Quantum Electron.* **2017**, *59*, 782–793. [CrossRef]
58. Gossard, E.E.; Hooke, W.H. *Waves in the Atmosphere*; Elsevier: Amsterdam, The Netherlands; New York, NY, USA, 1975; p. 456.
59. Grigoriev, G.I. Acoustic-gravity waves in the earth's atmosphere (Review). *Radiophys. Quanum Electron.* **1999**, *42*, 1–21. [CrossRef]
60. Offermann, D.; Jarisch, M.; Oberheide, J.; Gusev, O.; Wohltmann, I.; Russel, J.M., III; Mlynczak, M.G. Global wave activity from upper stratosphere to lower thermosphere: A new turbopause concept. *J. Atmos. Sol. Terr. Phys.* **2006**, *68*, 1709–1729. [CrossRef]
61. Tsuda, T.; Kato, S.; Yokol, T.; Inoue, T.; Yamamoto, M.; VanZand, T.E.; Fukao, S.; Sato, T. Gravity waves in the mesosphere observed with the middle and upper atmosphere radar. *Radio Sci.* **1990**, *26*, 1005–1018. [CrossRef]
62. Hines, C.O. Internal atmospheric gravity waves at atmospheric heights. *Can. J. Phys.* **1960**, *38*, 1441–1481. [CrossRef]
63. Grigor'ev, G.I.; Bakhmetieva, N.V.; Tolmacheva, A.V.; Kalinina, E.E. Relaxation time of artificial periodic irregularities of the ionospheric plasma and diffusion in the inhomogeneous atmosphere. *Radiophys. Quantum Electron.* **2013**, *56*, 187–196. [CrossRef]
64. Bakhmetieva, N.V.; Grigor'ev, G.I.; Tolmacheva, A.V.; Kalinina, E.E.; Egerev, M.N. Internal gravity waves in the lower thermosphere with linear temperature profile: Theory and experiment. *Radiophys. Quantum Electron.* **2017**, *60*, 103–112. [CrossRef]
65. Bakhmetieva, N.V.; Grigoriev, G.I.; Kalinina, E.E. Acoustic gravity waves with a heterogeneous temperature profile of the neutral component in the earth's atmosphere. *Russ. J. Phys. Chem. B* **2022**, *16*, 499–507. [CrossRef]
66. Tolmacheva, A.V.; Grigoriev, G.I. Polytropic Processes in the Lower Thermosphere. *Russ. J. Phys. Chem. B* **2021**, *15*, 582–589. [CrossRef]